AN ABSTRACT OF THE THESIS OF

Arien Sligar for the degree of Master of Science in Electrical and Computer Engineering presented on August 18, 2006.

Title: On-Chip Crosstalk Suppression Schemes using Magnetic Films for RF/Microwave Applications.

Abstract approved:

_____

Raghu K. Settaluri

The primary objective of the thesis research is to study novel schemes of on-chip crosstalk suppression employing magnetic films at microwave frequencies. Since extraction of various material properties of the magnetic films is essential for successful application of the proposed method, the research also involves development of a new material characterization technique using a grounded coplanar waveguide configuration.

The novel material characterization method allows simultaneous extraction of complex permeability, permittivity, saturation magnetization and resonance line-width of magnetic films for microwave applications. Material characteristics have been extracted from the full-wave EM simulations using only S-parameters for three different ferrite samples over the frequency range of 1 to 10 GHz for different applied external DC magnetic fields. The extracted parameters have been compared with the

input parameters as well as with the theoretical calculations based on previously reported research and were found to be in excellent agreement.

Crosstalk suppression is achieved by placing a magnetic film between circuit elements. A systematic study is carried out to determine the extent of crosstalk suppression for a variation in the material and physical characteristics of magnetic films using a pair of coupled microstrips. The results are validated by full-wave EM simulations as well as with measurement. Effectiveness of crosstalk suppression is presented in terms of S-parameters and fractional power coupled between the microstrips. The results indicate that an improvement of over 90% crosstalk reduction can be achieved with optimum material and physical properties.

On-Chip Crosstalk Suppression Schemes using Magnetic Films for RF/Microwave Applications

by
Arien Sligar

A THESIS

submitted to

Oregon State University

in partial fulfillment of
the requirements for the
degree of

Master of Science

Presented August 18, 2006
Commencement June 2007

Master of Science thesis of Arien Sligar presented on August 18, 2006

APPROVED:

Major Professor, representing Electrical and Computer Engineering

Director of the School of Electrical Engineering and Computer Science

Dean of the Graduate School

I understand that my thesis will become part of the permanent collection of Oregon State University libraries. My signature below authorizes release of my thesis to any reader upon request.

Arien Sligar, Author

TABLE OF CONTENTS

TABLE OF CONTENTS (Continued)

Page

LIST OF FIGURES

LIST OF FIGURES (Continued)

Figure Page

LIST OF FIGURES (Continued)

Figure Page

LIST OF TABLES

On-Chip Crosstalk Suppression Schemes using Magnetic Films for RF/Microwave Applications

1 Introduction

1.1 Background and Motivation

With increasing circuit density, higher speeds and miniaturization of electronics, crosstalk interference has become a major concern in LTCC (Low Temperature Co-fired Ceramic) and integrated circuit environments [1]. A limiting factor of many circuits is presented by electromagnetic noise introduced into the circuit from nearby components leading to unwanted electrical response deviations. Inductive and capacitive coupling resulting in unwanted noise between conductors is known as crosstalk. This unwanted noise, when large enough, can result in degradation of performance in a circuit. As feature size decreases, the need for an effective and more efficient crosstalk suppression scheme is evident.

1.2 Crosstalk Suppression Literature Review

Several methods are currently available to a designer to preserve signal integrity, including but no limited to differential signaling [2], guard traces [3]-[5], and substrate compensation [6]. These methods, although effective, can be limiting in there use. The first method to be discussed is the method of differential signaling in which immunity to crosstalk can be achieved by driving two closely spaced conductors 180 degrees out of phase, the signal can be extracted in a noisy environment due to both conductors experiencing the same noise. The signal integrity of differential conductors is excellent in exchange for a larger area occupied in

comparison with a single-ended line, as well as the addition of driving and receiving circuitry.

The use of guard traces is also a very effective crosstalk suppression method. Guard traces are typically used in a microstrip or stripline environment, where the grounded guard conductor is placed between two circuit elements as shown in Fig. 1.1. Reducing crosstalk between the circuit elements is achieved by effectively increasing the mutual capacitance between the guard trace and circuit element, and reducing the mutual capacitance between the circuit elements. Crosstalk as a result of inductive coupling can also be reduced by grounding both ends of the guard trace. With both ends of the guard trace grounded, a current in the reverse direction is induced in the guard trace as a result of Faraday's law. This induced current will in turn induce a current in the victim circuit element. The crosstalk in the victim line will then be the sum result of both the current induced by the guard trace, as well as the current induced by the aggressor line, both having opposite polarities. Implementation of a guard trace requires a minimum spacing between the guard trace and the circuit elements, if this minimum spacing is not maintained an additional coupling mode will be introduced and crosstalk will be increased [5].

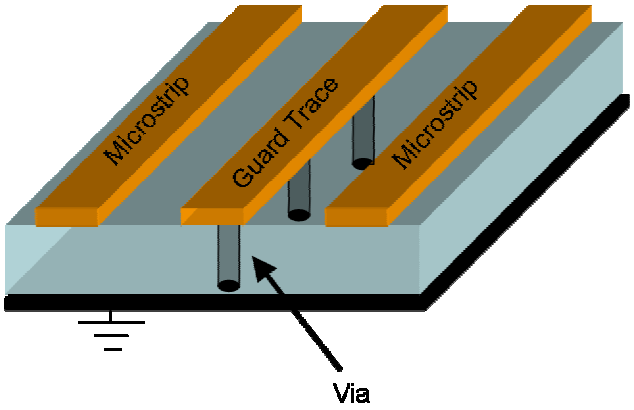

Fig. 1.1 Crosstalk suppression with the use of a guard trace with vias to ground, implemented in microstrip configuration.

The method of substrate compensation to reduce crosstalk is presented by the authors Gilb and Balanis [6]. A substrate with two layers of dielectric is used (Fig 1.2) to eliminate the far-end crosstalk by making the velocity of propagation of both even and odd mode to be equal. Although effective in reduction of far-end crosstalk, near-end crosstalk is not reduced. Complicated fabrication of multilayer dielectric substrates is also a major limitation of this method.

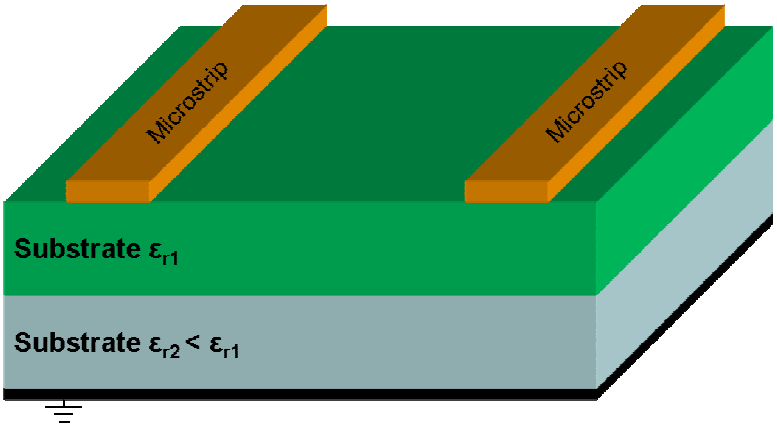

Fig. 1.2 The multilayered substrate shown here is used to suppress crosstalk through substrate compensation.

1.3 Crosstalk Suppression using Magnetic Films

In many RF circuits, crosstalk is introduced into the circuit when bus lines run long distances in parallel or when passive components such as spiral inductors, interdigital capacitors or even simple interconnects are placed in close proximity to each other, several examples are shown in Fig. 1.3. The approach presented here to reduce crosstalk uses the application of a magnetic film/ferrite in the area separating two closely spaced circuit elements. This effectively reduces the crosstalk as a result of inductive coupling of circuit elements through the lossy properties of magnetic materials during ferromagnetic resonance (FMR).

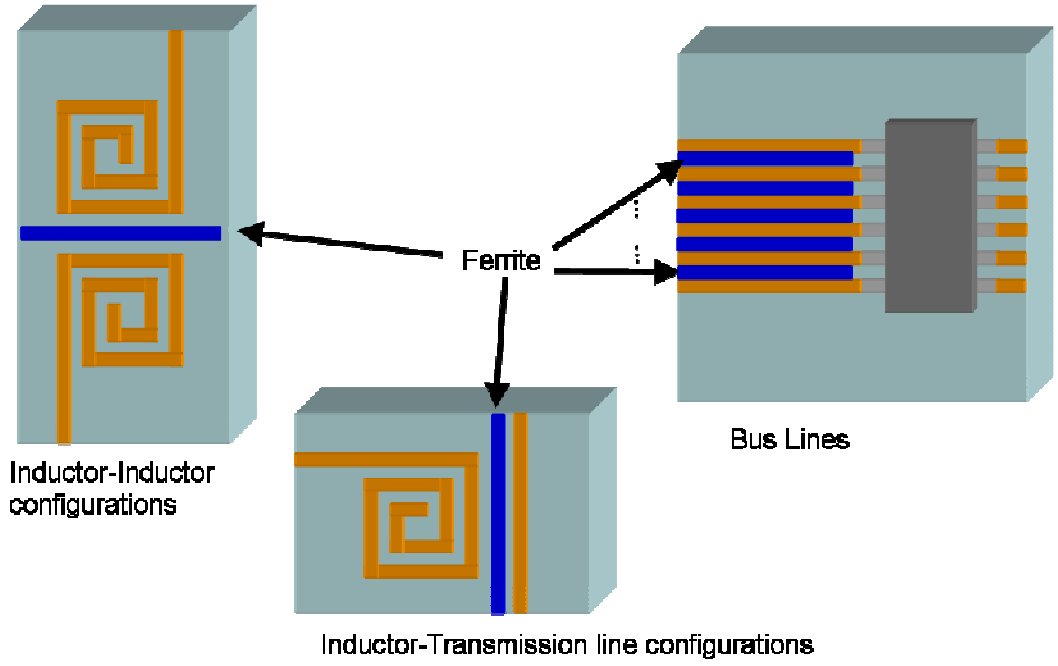

Fig. 1.3 The suppression of crosstalk using magnetic films has applications in areas such as closely spaced inductors, transmission lines near inductors and in bus lines. The magnetic film is placed between the circuit elements where isolation is required.

Prior research reported application of magnetic films on the surface of the circuit elements to prevent radiation of high frequency noise [7]-[13]. This technique primarily focuses on eliminating the radiation by increasing the insertion loss in the stop band, where signals need to be attenuated. The primary goal of these methods is to reduce radiated noise harmonics outside the band of operation. This techniques is not particularly suitable for crosstalk suppression due to high insertion losses when a magnetic material is placed directly above circuit elements. Novel crosstalk suppression schemes that can offer simpler implementation with predictable frequency response will be of great interest to the industry as well as to the research community.

1.4 Material Characterization

The knowledge of several material properties of the magnetic film is required in order to be properly implemented into this crosstalk suppression method. This work presents a broadband method, in which material properties essential to crosstalk suppression can easily be extracted simultaneously at microwave frequencies using a network analysis. While numerous methods to extract material properties exist, the method developed here is highly suitable to characterize the material for application to crosstalk suppression.

1.5 Thesis Organization

This thesis is organized into two major sections; material characterization and crosstalk suppression using magnetic films. In chapter 2, the method in which

magnetic materials can be characterized over microwave frequencies using a grounded coplanar waveguide is described. Three examples showing the extraction of complex permittivity and permeability from 1 GHz to 10 GHz is shown for demagnetized materials. This is followed by a demonstration in extracting the saturation magnetization, ferromagnetic line-width and complex permeability of the same three materials with DC magnetic field applied to magnetize the material. The second topic on crosstalk suppression is discussed in chapters 3 and 4. Chapter 3 presents the theory behind the crosstalk suppression as well as full-wave EM simulations that validate the theory. It also presents discussions on the effect of material properties as well as placement of the magnetic films for best performance. Chapter 4 continues the topic of crosstalk suppression with measurement results of two fabricated circuits. These measurement results further validate the theory described in chapter 3 as well as prove how crosstalk can effectively be reduced in 'real world' applications with magnetic films.

As a final chapter in this thesis, a conclusion is drawn from the results presented. Also, suggestions are made as to where this research may lead and possible avenues to be explored that may result improvements to the work presented here.

2 Material Characterization

2.1 Introduction

Microwave circuits such as isolators, circulators, phase shifters, tunable resonators and filters commonly use magnetic materials and require knowledge of several material properties such as complex permittivity, complex permeability, saturation magnetization and ferromagnetic resonance (FMR) line-width [14]. In the past, several researchers have reported measurement based techniques for the extraction of material properties [15]-[22]. Primarily, these methods are based on either the transmission/reflection method [15]-[20] or the inductive method [21], [22] to determine the material properties. The inductive method uses either the transmission or the reflection coefficient to relate the inductance of the transmission line to the permeability of the material. Determination of electrical properties such as permittivity can not be determined using this technique. The transmission/reflection method uses both the transmission and reflection coefficients to relate the characteristic impedance and propagation constant to the permeability and permittivity. Many of the current transmission/reflection techniques do not allow determination of these properties near resonance due to the frequency sensitive nature of the complex permeability and often, the limitation associated with the filling factors [15].

An accurate technique for broadband extraction of the complex permeability and permittivity from S-parameter data is presented in this chapter. The choice of the

homogeneous grounded coplanar waveguide (GCPWG) geometry and the extraction procedure allows accurate extraction of these parameters even at ferromagnetic resonance. This thesis also presents a novel means of determination of saturation magnetization and resonance line-width from the extracted complex permeability and the resonance frequency.

2.2 Grounded Coplanar Waveguide

Figure 2.1 shows a GCPWG configuration, homogeneously filled with an unknown material, for which the material characteristics need to be determined. A grounded conductor is placed on both the top and the bottom of the waveguide. The conductor width and the spacing between conductors are chosen to be sufficiently smaller than half a wavelength to insure that the structure supports a TEM mode of propagation [16], [23], [24]. The length of the transmission line is also chosen to be less than half a wavelength to avoid any ambiguity in terms of the electrical delay.

Many of the planar techniques using the transmission/reflection method cannot accurately extract the permeability over large changes in magnitude [15], such as during ferromagnetic resonance. This limitation arises during the derivation of permeability, in which conformal mapping is used to calculate the filling factors. The filling factors are used to separate out the inhomogeneous media, such as air or the known substrate from the material which is to be characterized. The homogenous filling material along with the top and bottom ground planes eliminates the need for filling factors and thus permeability can accurately be determine over FMR.

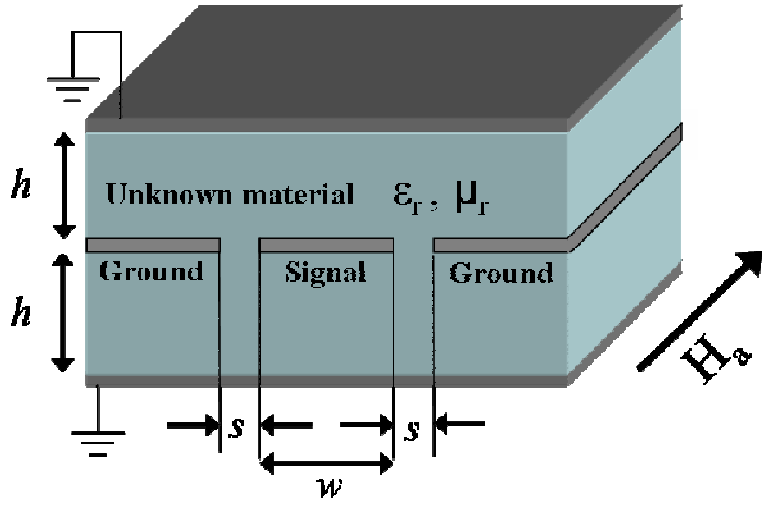

Fig. 2.1 A homogeneously filled GCPWG configuration for the extraction of ε, μ, $4\pi Ms$ and ΔH. Dimensions: h = 30 μm, s = 25 μm, and w = 100 μm. Externally applied magnetic field applied longitudinally given as H_a.

2.3 Theory

After obtaining the scattering parameters of the test structure from measurement/full-wave electromagnetic simulation, they are first converted to ABCD parameters. In this chapter, the frequency dependent S-parameters are determined from commercially available FEM full-wave EM simulation software (Ansoft HFSS 9.2) for faster verification of this technique over a wide range of material properties without the need for fabrication. This procedure can be easily extended to measurement based characterization, where the scattering parameters are available from experimental data for the homogeneously filled structure. The ABCD parameters for the GCPWG structure of length l can be expressed in terms of the propagation parameters of the transmission line as

$$\begin{bmatrix} A & B \\ C & D \end{bmatrix} = \begin{bmatrix} \cosh(\gamma l) & Z_c \sinh(\gamma l) \\ \dfrac{\sinh(\gamma l)}{Z_c} & \cosh(\gamma l) \end{bmatrix} \tag{2.1}$$

where Z_c, and γ are the characteristic impedance and the propagation constant of the transmission line respectively. From (2.1), the characteristic impedance and propagation constant can be expressed in terms of the known ABCD parameters and the length of the coplanar waveguide [25]. An ambiguity does result in the propagation constant due to electrical length being an unknown, but can be resolved by keeping the length of the GCPWG to less than half a wavelength long.

The characteristic impedance and the propagation constant can also be expressed as (2.2) and (2.3) [17], [18].

$$Z_o = Z_a \sqrt{\frac{\mu_r}{\varepsilon_r}} \tag{2.2}$$

$$\gamma = \omega \sqrt{\varepsilon_o \mu_o} \sqrt{\varepsilon_r \mu_r} \tag{2.3}$$

where Z_a is the characteristic impedance when the filled material is replaced with free space ($\varepsilon_0 = 8.854*10^{-12}$ F/m, $\mu_0 = 4\pi*10^{-7}$ H/m) and ω, ε_r and μ_r are angular frequency, relative permittivity and relative permeability, respectively. The frequency dependent characteristic impedance when the filling material is replaced by free space, while keeping the dimensions the same, can be determined through simulation, measurement or conformal mapping techniques.

Equations (2.2) and (2.3) can be re-arranged as shown in (2.4) and (2.5) to determine the complex permeability and permittivity of the unknown material.

$$\varepsilon_r = \varepsilon' - j\varepsilon'' = \frac{Z_a \gamma}{\omega Z_o \sqrt{\varepsilon_o \mu_o}} \tag{2.4}$$

$$\mu_r = \mu' - j\mu'' = \frac{Z_o \gamma}{\omega Z_a \sqrt{\varepsilon_o \mu_o}} \tag{2.5}$$

Since the proposed procedure does not involve any constraints on the material parameters or requires definition of any filling factors, it would also be valid when an external DC longitudinal magnetic field, H_a is applied to excite ferromagnetic resonance in the structure. This enables us to propose a novel means of determining the saturation magnetization, $4\pi M_s$ and resonance line-width, ΔH from the frequency dependent behavior of the complex permeability shown in (2.5). For this, an external DC field, sufficiently larger than the field attributed to any anisotropy fields of the sample and large enough to ensure single domain structure of the magnetic material is applied to the structure such that it results in a ferromagnetic resonance in the frequency band of interest. The ferromagnetic resonant frequency, f_{res} can be extracted from the imaginary part of the frequency sensitive permeability. Rearranging Kittel's condition for resonance [26], the saturation magnetization can be determined as shown in (2.6).

$$4\pi M_s = \frac{f_{res}^2}{\gamma_{gyro}^2 H_a} - H_a \tag{2.6}$$

where, H_a is the applied external DC magnetic field and γ_{gyro} is the gyromagnetic ratio. The gyromagnetic ratio will be approximated as 2.8 MHz/Oe,

which is an accurate estimate for most ferrite materials [27]. The FMR line-width, ΔH can be determined using (2.7), where f_2 and f_1 are frequencies at which, μ'' is equal to half the maximum value.

$$\Delta H = \frac{(f_2 - f_1)}{\gamma_{gyro}} \tag{2.7}$$

2.4 Simulation Results

The proposed technique is validated by examining the accuracy of the extracted material properties for three different ferrite materials with properties comparable to magnesium ferrite, lithium ferrite and nickel ferrite. Using full-wave electromagnetic simulations to determine the frequency dependent scattering parameters of the structure with these material parameters entered into the simulator. Using the procedure described in section 2.32, material properties have been extracted and compared with those entered into the simulator. First intrinsic material properties from the material in a completely demagnetized state are extracted. This completely demagnetized state allows for extraction of intrinsic permittivity and permeability of the material. Applying an external static field in the longitudinal direction, saturation magnetization, FMR line-width, permittivity and the diagonal components of the permeability tensor can then be extracted for the sample in a magnetized state.

2.4.1 Intrinsic Material Properties

First, a material similar to magnesium ferrite is considered with ε_r = 12.9-j0.00645, μ_r = 25+j0, $4\pi M_s$ = 3000 Gauss and ΔH = 200 Oe. Figure 2.2 shows the extracted values of ε' and μ' of the sample in a completely demagnetized state with no externally applied field. The extracted results are accurate to within 2% when compared to the known input values. Values of ε'' and μ'' are relatively constant at 6.25 x10^{-3} and 10^{-4} respectively. It may be noted that the frequency dependence of the permittivity and permeability is not evident, when the magnetic material is considered demagnetized. This is due to the intrinsic values entered into the simulator are considered to be a constant value over all frequencies. This is not the case for the magnetized material as it will be seen in section 2.4.2.

As a second example, a material with similar properties to a lithium ferrite with ε_r = 16.5-j0.0165, μ_r = 50, $4\pi M_s$ = 1700 Gauss and ΔH = 400 Oe is used. The complex permittivity and permeability were extracted by considering a demagnetized sample and are found to be accurate within 1.5% of the input values. The resulting extracted values are shown in Fig. 2.3.

The demagnetized sample comparable to nickel with ε_r = 13-j0.0195, μ_r = 300, $4\pi M_s$ = 5000 Gauss and ΔH = 165 Oe is considered as a third example. In the demagnetized state, the permittivity and permeability were extracted to be accurate within 2%. The permittivity and permeability extracted from the HFSS simulations are shown in Fig. 2.4.

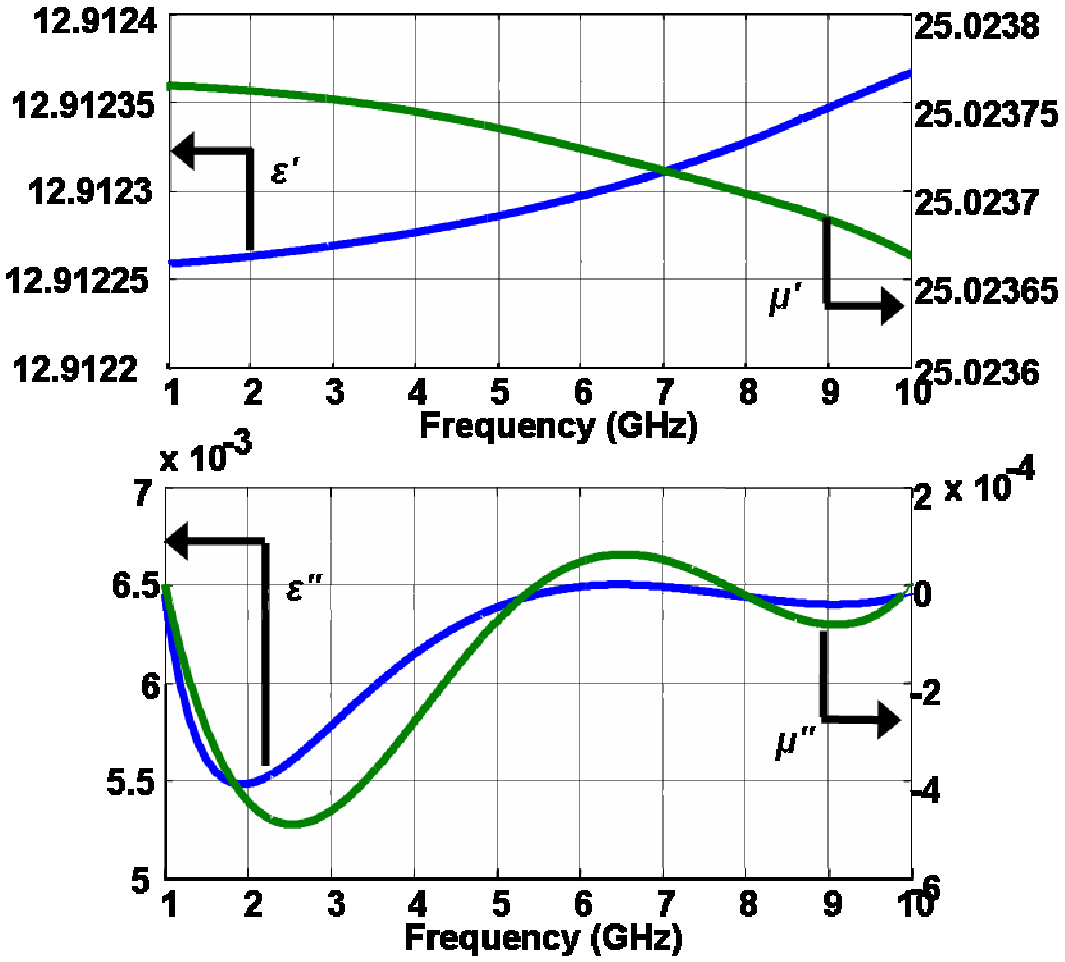

Fig. 2.2 Extracted results for ε and μ. Input values are: $\varepsilon' = 12.9$, $\varepsilon'' = 0.0065$, $\mu' = 25$, $\mu'' = 0$.

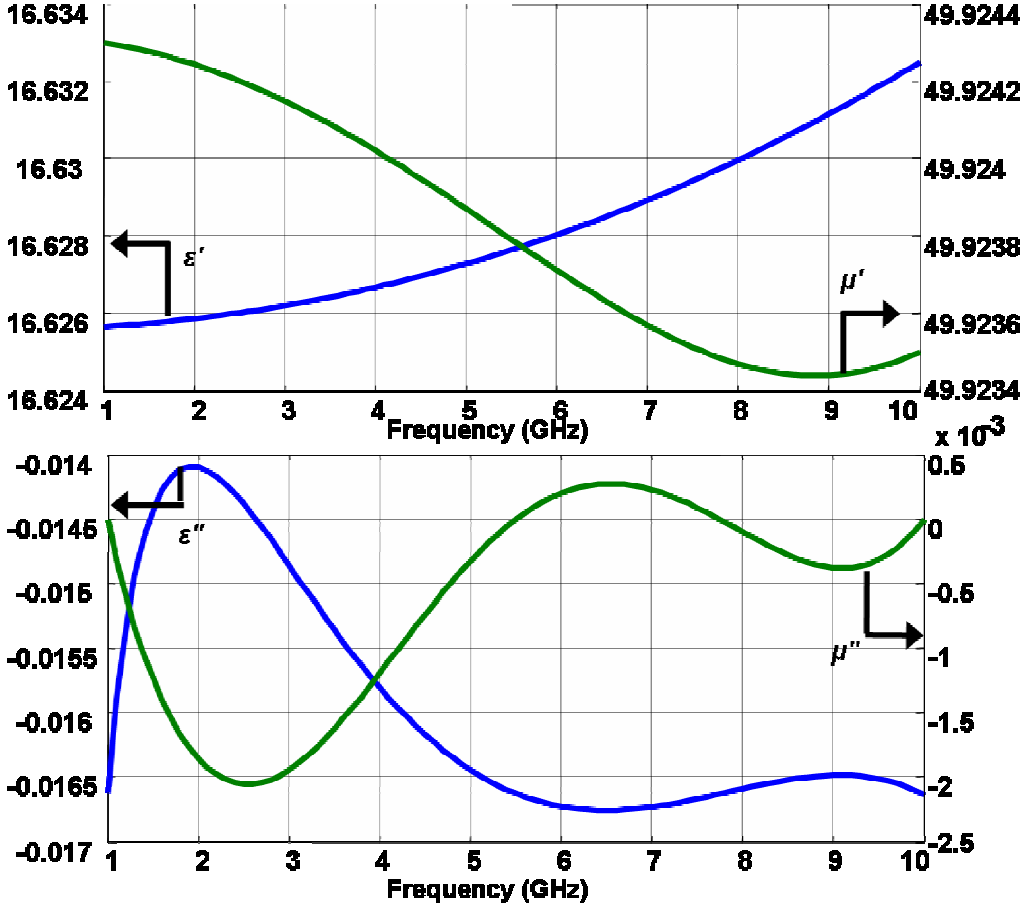

Fig. 2.3 Extracted results for ε and μ. Input values are: $\varepsilon' = 16.5$, $\varepsilon'' = 0.0165$, $\mu' = 50$, $\mu'' = 0$.

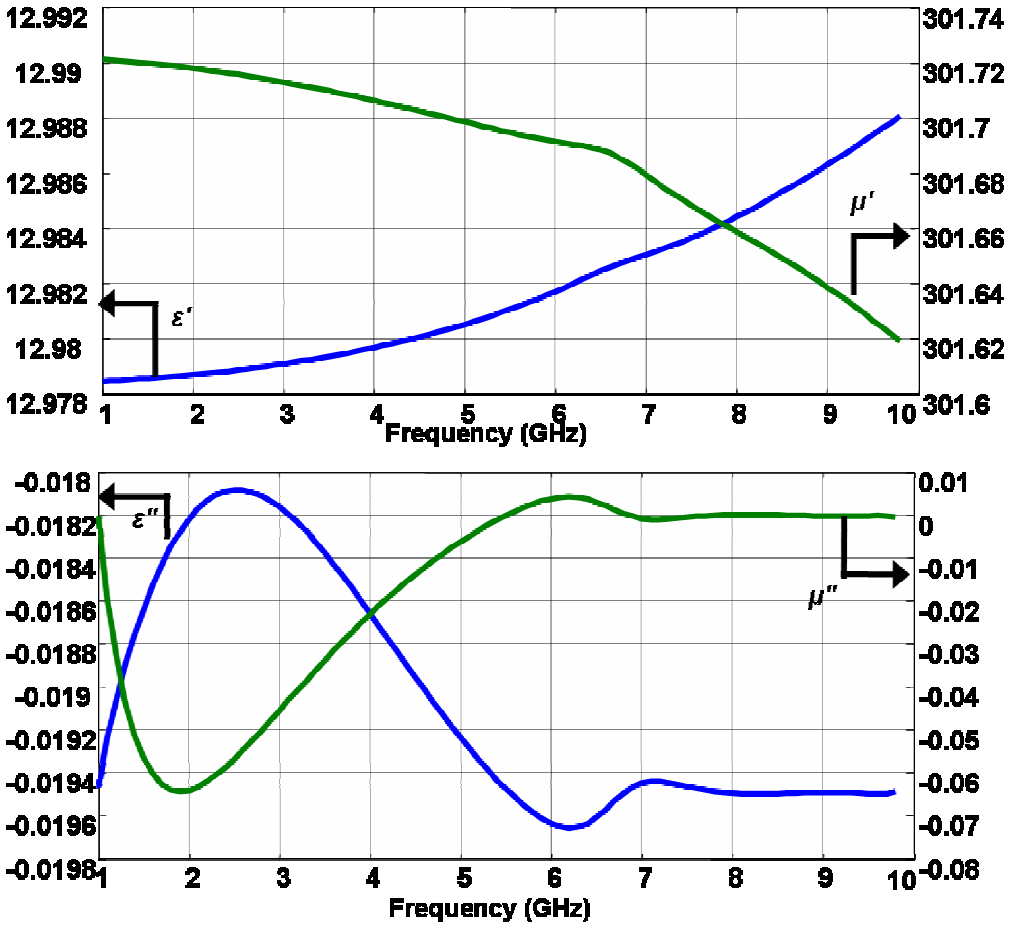

Fig. 2.4 Extracted results for ε and μ. Input values are: $\varepsilon' = 13$, $\varepsilon'' = 0.0196$, $\mu' = 300$, $\mu'' = 0$.

2.4.2 Magnetized Material Properties

Of more significance to the design of microwave components and crosstalk suppression is the material behavior when the sample is magnetized. As a magnetic material is subjected to a static magnetic field, the permeability is of most interest, considering the dielectric properties of the material remain relatively unchanged. The permeability is now dependant on several factors including the saturation magnetization, FMR line-width and applied static magnetic field.

Again considering the Magnesium ferrite (ε_r = 12.9-j0.0645, μ_r = 25+j0, $4\pi M_s$ = 3000 Gauss and ΔH = 200 Oe) now magnetized with an external magnetic field applied in the longitudinal direction. Fig. 2.5 shows the frequency response of the real and imaginary parts of the diagonal components of the permeability tensor for the Magnesium Ferrite sample with three different values of externally applied field, 600 Oe, 800 Oe and 1000 Oe. The external DC magnetic field will be considered equal to the total internal field minus shape anisotropy field as other anisotropy fields are not considered in HFSS. For validation, the theoretical permeability (2.8) derived by Spenato *et al.* [28] for films with in-plane uniaxial anisotropy and a perpendicularly applied alternating magnetic field is also plotted in Fig. 2.5.

$$\begin{aligned}\mu = \mu' - j\mu'' = &\left[\gamma_{gyro}^2 4\pi M_s\left(H_k + 4\pi M_s\right) + jf\alpha 4\pi M_s\right]... \\ &\times\left[-f^2\left(1-\alpha^2\right)^2 - f^2\alpha^2 + \gamma_{gyro}^2 H_a\left(H_k + 4\pi M_s\right) - jf\alpha\gamma_{gyro}\left(2H_k + 4\pi M_s\right)\right]... \\ &\times\left\{\left[-f^2\left(1-\alpha^2\right)^2 - f^2\alpha^2 + \gamma_{gyro}^2 H_a\left(H_k + 4\pi M_s\right) + jf\alpha\gamma_{gyro}\left(2H_k + 4\pi M_s\right)\right]^2...\right. \\ &\left.+ f^2\alpha^2\gamma_{gyro}^2\left(H_k + 4\pi M_s\right)^2\right\}^{-1} + 1\end{aligned} \tag{2.8}$$

where α is the Gilbert damping constant shown in (2.9), H_k is the anisotropy field and f is the frequency of the applied magnetic field.

$$\alpha = \frac{\Delta H \gamma_{gyro}}{2 f_{res}} \tag{2.9}$$

It may be noted that the theoretical response matches very closely with the values extracted from this procedure. The behavior of the extracted values is also in strong agreement with the Stoner-Wohlfarth theory [29]. For example, the

extrapolation of the real portion of the permeability to DC is in close agreement with the expected value of $\mu'=4\pi M_s/H_a+1$. Also, it can be seen that the maximum value of μ'' decreases as the externally applied field increases. A summary of extracted results for the Magnesium ferrite is shown in Table 2.1. For all three applied fields, the extracted values of $4\pi M_s$ are within 1% accuracy compared to the theoretical values. Extracted values of ΔH are in close agreement with theoretical values as per [28], and as expected, the resonance line-width approaches the specified input value for large values of applied external field [30].

The Lithium ferrite (ε_r= 16.5-j0.0165, μ_r= 50, $4\pi M_s$ = 1700 Gauss and ΔH = 400 Oe) is now magnetized by applying a longitudinal static magnetic field. Fig. 2.6 shows the extracted permeability in comparison with the theoretical permeability computed from [28] for three different values of externally applied field. When the applied field was 600 Oe, a slight disagreement can be seen in the real part of the permeability. This could possibly be due to the shape anisotropy field being relatively large with respect to the saturation magnetization as compared to the last example. A summary of extracted values for three different applied fields is given in Table 2.2.

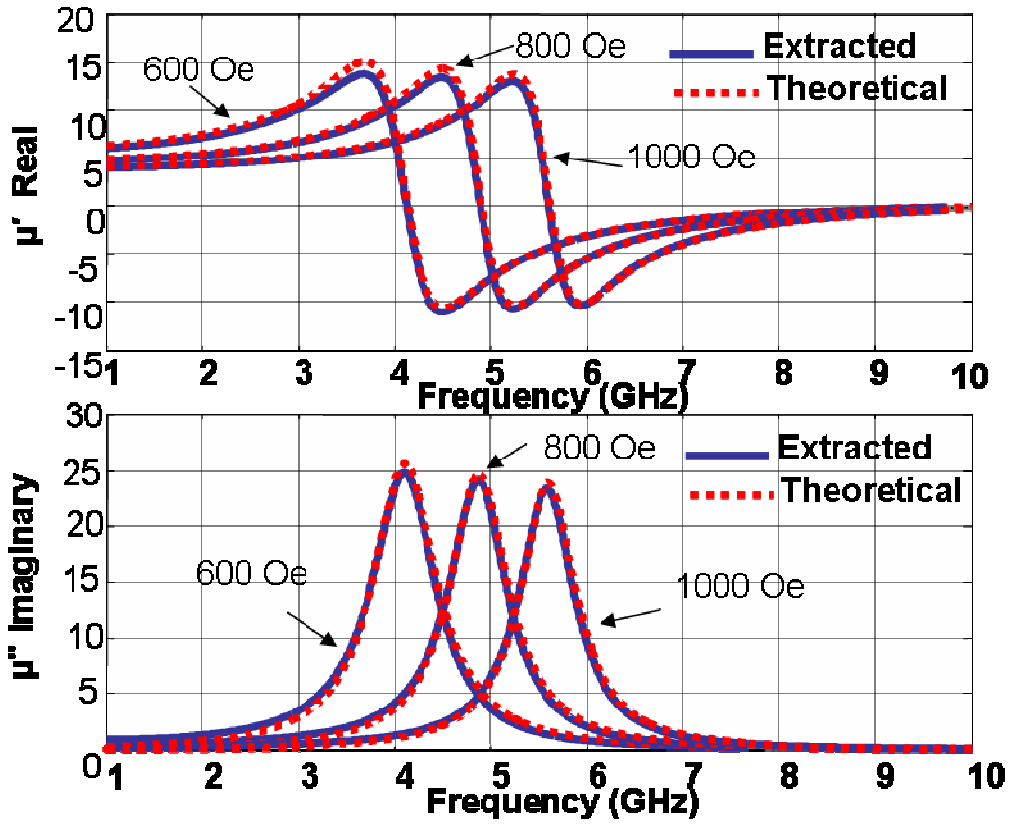

Fig. 2.5 Extracted and theoretical values of μ, for external applied fields (H_a) of 600, 800 and 1000 Oe for the Magnesium ferrite sample.

Table 2.1 Extracted saturation magnetization and resonance line-width for magnesium ferrite

H_a (Oe)	$4\pi M_s$ (G) (Extracted)	% Error	ΔH (Oe) (Extracted)	ΔH (Oe) (Theoretical)	% Error
600	2973.6	0.88%	292.86	289.28	1.23%
800	2981.4	0.62%	264.28	267.86	1.34%
1000	2985.7	0.48%	250	253.57	1.40%

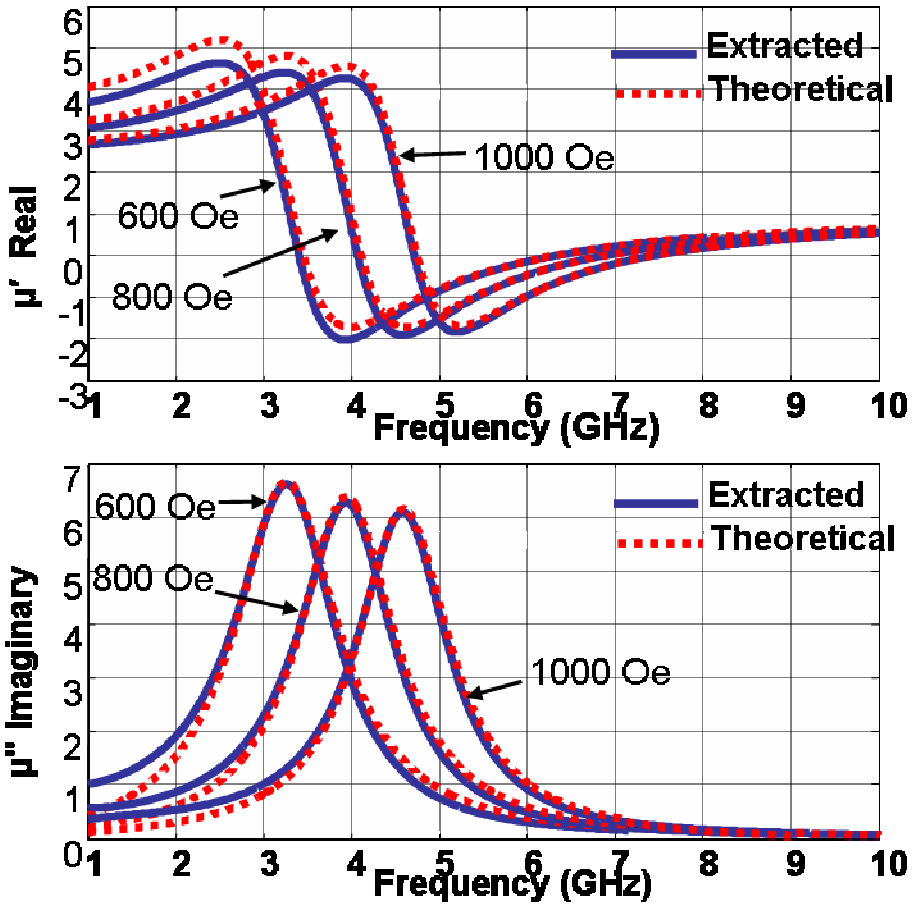

Fig. 2.6 Extracted and theoretical values of μ, for external applied fields (H_a) of 600, 800 and 1000 Oe for the Lithium ferrite sample.

Table 2.2 Extracted saturation magnetization and resonance line-width for lithium ferrite

H_a (Oe)	$4\pi M_s$ (G) (Extracted)	% Error	ΔH (Oe) (Extracted)	ΔH (Oe) (Theoretical)	% Error
600	1667.4	1.92%	510.7	507.1	0.71%
800	1683.9	0.95%	478.6	475.0	0.76%
1000	1685.1	0.87%	458.0	457.1	0.20%

As a final example of extraction of material properties from a magnetized sample, Nickel ferrite (ε_r = 13-j0.0195, μ_r = 300, $4\pi M_s$ = 5000 Gauss and ΔH = 165

Oe) is again considered. The results agree very well both with Stoner-Wohlfarth theory and Spenato's theoretically derived permeability. A response of the complex permeability for different values of applied external field is shown in Fig. 2.7. The extracted values of saturation magnetization and the resonance line-width for different cases are shown in Table 2.3. It may be seen that, for this example, the extracted values are in excellent agreement with the theoretical values computed from [28].

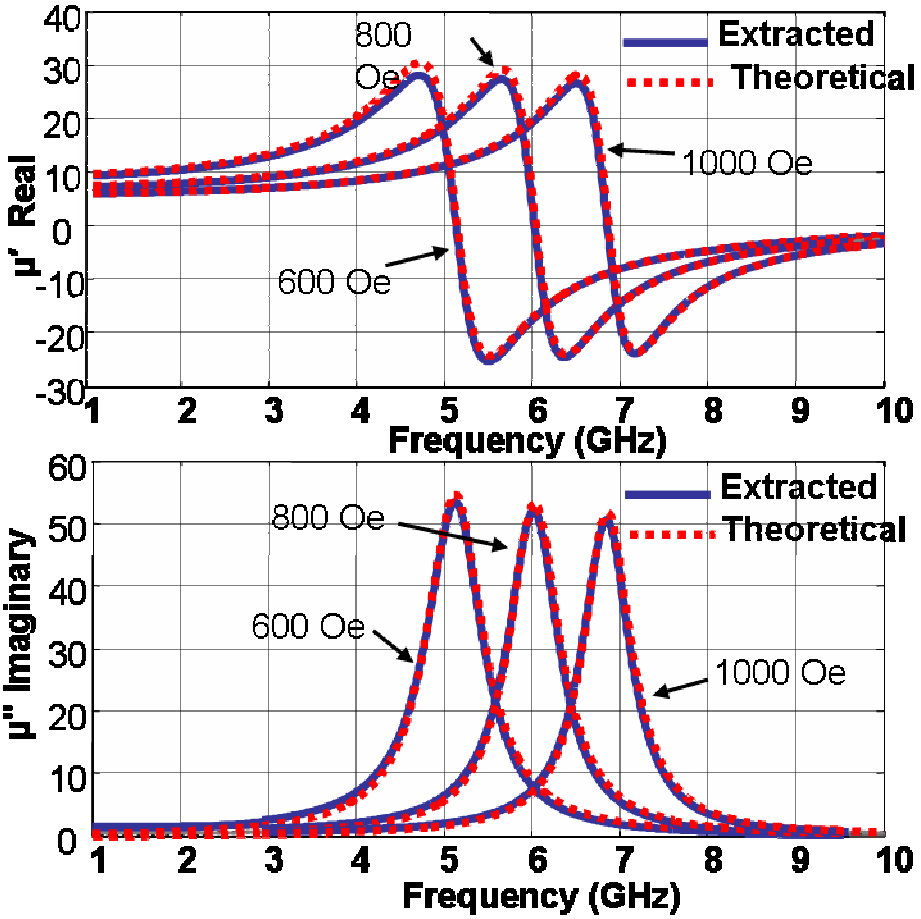

Fig. 2.7 Extracted and theoretical values of μ, for external applied fields (H_a) of 600, 800 and 1000 Oe for the Nickel ferrite sample.

Table 2.3 Extracted saturation magnetization and resonance line-width for nickel ferrite

H_a (Oe)	$4\pi M_s$ (G) (Extracted)	% Error	ΔH (Oe) (Extracted)	ΔH (Oe) (Theoretical)	% Error
600	4992.7	0.15%	278.57	278.57	0%
800	4998.8	0.02%	253.57	253.57	0%
1000	4989.9	0.22%	239.29	239.29	0%

2.5 Conclusion

A novel technique for broadband extraction of various important material characteristics of film magnetic materials is presented in this chapter. The extracted complex permittivity and permeability for different demagnetized ferrite samples are found to be accurate within 2% of the input values. This chapter also describes a procedure to extract the saturation magnetization and resonance line-width from the complex permeability of the magnetized ferrite samples. For all examples, the extracted values matched very closely with the behavior predicted by the theory of Stoner-Wohlfarth and derived permeability of Spenato.

3 Crosstalk Suppression Employing Magnetic Films

3.1 Introduction

With the increasing speeds of operation and shrinking package sizes, crosstalk is considered as one of the most important design aspects to many engineers. The effect of crosstalk can often be difficult to predict and include in the design. The current methods [3]-[8] can frequently be limiting and may not be realizable in the given circuit. This chapter presents a new technique for crosstalk suppression, in which a magnetic film is deposited between circuit elements to reduce crosstalk. The new method can offer potential advantages compared to some of the other available options.

3.2 Test Structure

As in many cases, crosstalk is introduced into circuits through interconnects running long distances in close proximity to each other or even when passive components are closely spaced. The crosstalk effect is generally predominant in interconnects which are close to each other. Therefore, a logical test structure to study the crosstalk suppression is a pair of coupled microstrip interconnects shown in Fig. 3.1. With the coupled interconnects realized in microstrip configuration, the effect of employing the magnetic material to suppress the near-end crosstalk (NEXT) and the far-end crosstalk (FEXT) without significantly affecting the through-port insertion loss (IL) and return loss (RL) of the structure is studied. Frequency dependant scattering parameters will be analyzed to verify the effectiveness of the crosstalk

suppression. The analysis of the 4-port network used in this crosstalk suppression scheme will be simplified by assuming the pair of coupled microstrips will only be driven at one port. This effectively reduces the number of scattering parameters observed from 16 to 4 and adding the assumption that the crosstalk suppression will be unidirectional. When driving port 1, as shown in Fig. 3.1, the scattering parameters S_{31} and S_{41} will be used to denote NEXT and FEXT, respectively. Insertion loss will be given as S_{21} and return loss as S_{11}. The test structure is shown in Fig. 3.1, which is designed on a dielectric substrate with thickness 200 μm and a relative permittivity of 12. The two 50 ohm microstrips are spaced 300 μm apart, with a width of 129.9 μm and thickness of 4 μm. Without the crosstalk suppression mechanism, this configuration results in a coupling of the order of -25 dB on the far-end port and -20 dB on the near-end port at 5 GHz as shown in Fig. 3.2. Insertion loss and return loss is shown in Fig. 3.3 for the coupled microstrips with no magnetic film.

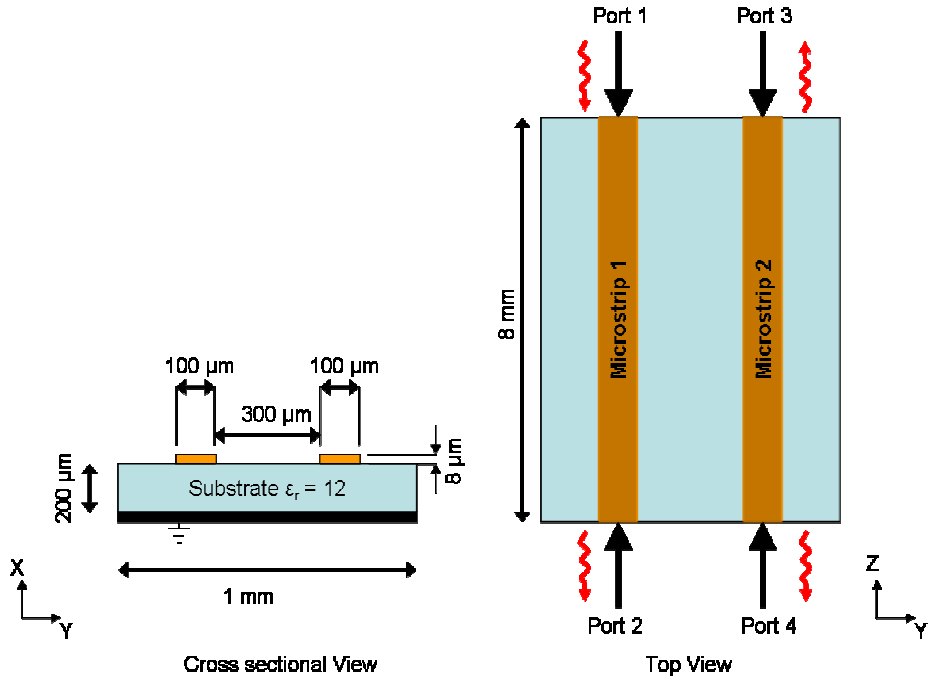

Fig. 3.1 A pair of coupled interconnects without a magnetic film to be used as a test structure to determine the effectiveness of this crosstalk suppression method.

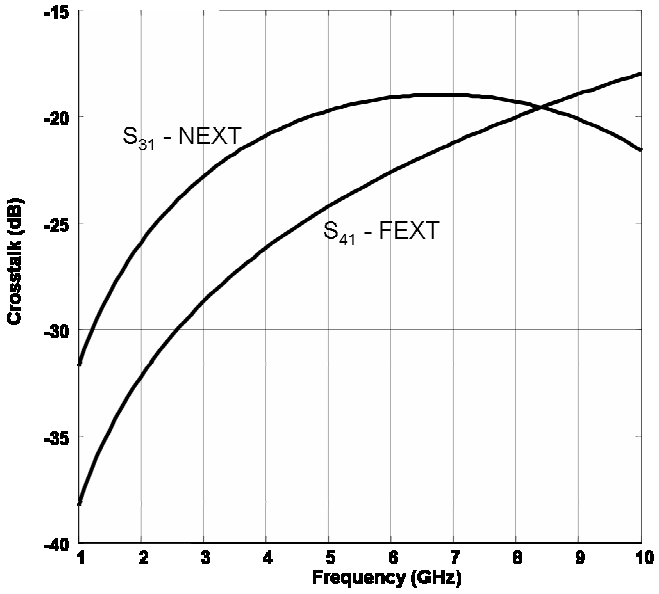

Fig. 3.2 Scattering parameter frequency response of test structure shown in Fig. 3.1 for near-end and far-end crosstalk.

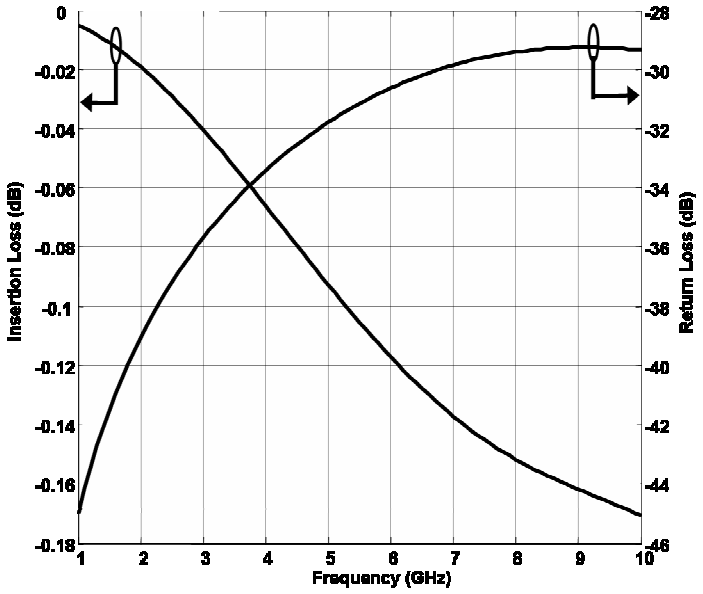

Fig. 3.3 Scattering parameter frequency response of test structure shown in Fig. 3.1 for insertion loss, shown on the left axis, and return loss shown on the right axis.

For crosstalk suppression, we propose to introduce a magnetic film in the space between the two microstrips as shown in Fig. 3.4. It will be demonstrated that the near-end and the far-end crosstalk of the coupled interconnect configuration can be varied by changing the physical properties such as offset from the center (G), width (W), length (L) and thickness (t), as well as the material properties of the magnetic film. The distance, G, will be assumed to be a positive number when the offset is toward microstrip 2 and port numbering is consistent with of those given in Fig. 3.1. The direction of internal static magnetic field (H_o) will always be applied in the direction shown in Fig. 3.4. For a given interconnect configuration, the optimum position of the film can be determined based on the desired crosstalk suppression and maximum allowable through-port insertion loss.

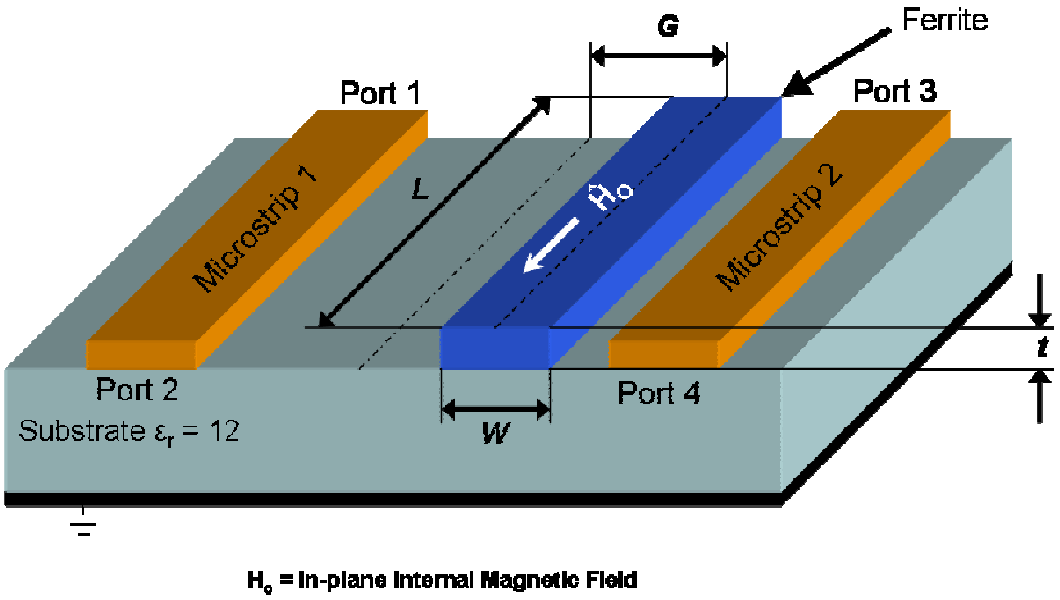

Fig. 3.4 Test structure shown in Fig. 3.1 with the addition of a magnetic film to aid in the suppression of crosstalk. Physical properties of the magnetic film will be given in terms of *W*, *L*, and *t*. Placement of the magnetic film will be described in section 3.5.1.

3.3 Theory

With the addition of a magnetic material in the space between the two microstrips in the test structure, the effectiveness of crosstalk reduction can be observed. Since the primary objective is to decrease the coupling between circuit elements, magnetic materials with high losses at the microwave frequency of interest are desirable.

Using a magnetic material that is going to have a strong and lossy interaction with the magnetic field generated by a microstrip, we can expect inductive coupling to be reduced between the two microstrips. This interaction is primarily a result of ferromagnetic resonance (FMR). Although magnetic materials mainly exhibit losses

using two mechanisms viz., eddy current losses and ferromagnetic resonance [31], the eddy current losses can be considered to be relatively small in comparison with the losses associated with FMR [12]. Electric losses, resulting in reduction of capacitive coupling can be seen with increased levels of conductance, but in comparison to the magnetic losses they are relatively small [32].

3.3.1 Ferromagnetic Resonance

The strong interaction between the magnetic moment of a magnetic dipole and an applied alternating magnetic field is known as ferromagnetic resonance. Looking first at the behavior of a single magnetic dipole, it can be seen in Fig. 3.5a that as a static magnetic field is applied to the magnetic dipole, a precession about the axis of the applied field occurs in the direction shown. The total magnetization can be thought of as the sum result of all the single magnetic dipoles of the material.

In the absence of an RF magnetic pumping field to sustain this precession, losses will cause this rotation to eventually spiral in to alignment with the direction of the static magnetic field axis as shown in Fig. 5.5b. This damping term, α, is related to the FMR line-width discussed in chapter 2 by (2.9). Applying an RF magnetic field that has components in the plane normal to the static applied field, a pumping action can occur in which the precession of the magnetic dipoles will be maintained. This RF applied field will have the strongest interaction when its frequency is at f_{res}, as given in (3.1) and having a circular polarization in the same sense as the rotating magnetic dipole shown in Fig. 3.5c. The result of this interaction between the RF magnetic field and the magnetic dipoles is high absorption of the magnetic field.

Energy absorption occurs in the form of radiated heat from the magnetic material. RF magnetic fields rotating in the opposite direction have a relatively small interaction and pass through the magnetic material with very little loss.

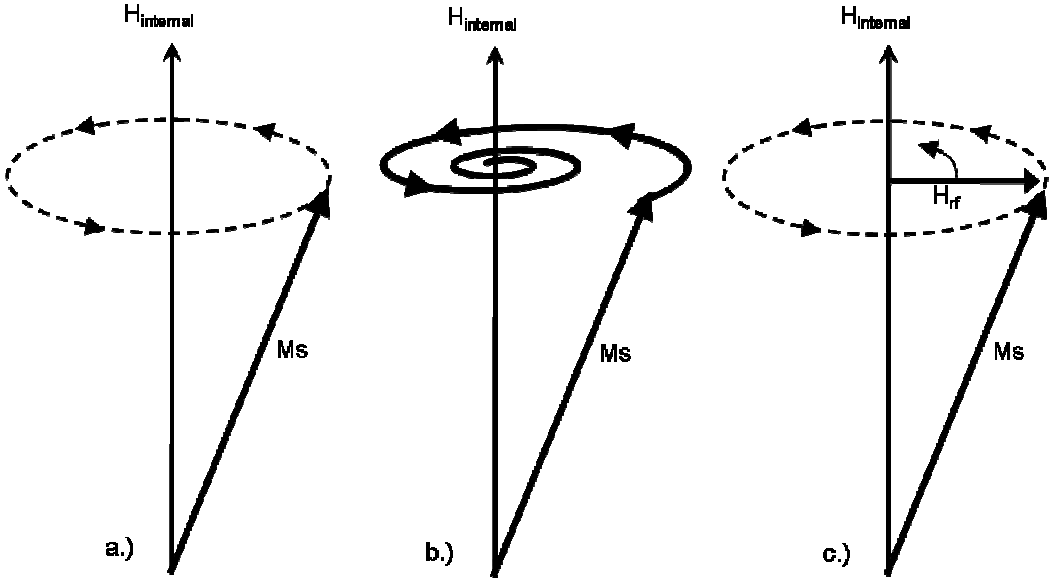

Fig. 3.5 a.) The precession of a magnetic moment caused by the static magnetic field applied in the absence of any loss mechanisms. b.) Damping caused by friction causes magnetic moment to align with static magnetic field. c.) Pumping action caused by an in plane RF magnetic field

The circuit topology of a microstrip results in an elliptical polarization of the magnetic field at the surface of the substrate near a microstrip. Although the polarization is not circular, interaction between the magnetic moments in the ferrite and elliptically polarized RF magnetic fields will still have a strong interaction. The RF field direction of rotation is dependent on which port is being driven and on which side of the microstrip is being observed. For example, at the substrate surface of a microstrip line, an elliptically polarized magnetic field will be present on both sides of the microstrip rotating in opposite direction. This leads to the understanding that

crosstalk suppression will not be reciprocal between to closely spaced microstrip transmission lines.

The frequency in which the dipole rotates in a finite shape has been discussed in detail by Kittel [26] and the resulting condition for resonance is given in (3.1).

$$f_{res} = \gamma_{gyro}\sqrt{[H_o + (N_y - N_z)4\pi M_s][H_o + (N_x - N_z)4\pi M_s]} \quad (3.1)$$

where,

$$H_o = H_k - 4\pi M_s\left(N_z - N_y\right) \quad (3.2)$$

$$N_z = \frac{2t}{\pi L} \quad (3.3)$$

$$N_y = \frac{2t}{\pi W} \quad (3.4)$$

$$N_x = 1 - \left(N_z + N_y\right) \quad (3.5)$$

Where, $4\pi M_s$ is the saturation magnetization, γ is the gyromagnetic ratio (2.8 MHz/Oe), H_o is the total internal magnetic field, which is equal to the sum of all the anisotropy fields as shown in (3.2). N_x, N_y and N_z are the demagnetization factors in the respective directions. In these equations, t is the thickness, L is the length, and W is the width of the magnetic film in microns. The original expressions for the demagnetization factors have been given in [33] for the magnetic film with uniform internal field. Those equations are considered to be valid as long as the thickness of the magnetic film, t is much smaller than other dimensions.

3.4 Criteria for Choosing Material

Microwave ferrites are typically available with a very large range of material properties [27]. Permittivity is typically in the range from 10 to 20 with dielectric loss tangents of the order of 10^{-4}. Intrinsic permeability can range from less than 10 to several thousand. Saturation magnetizations are available to well over 8000 Gauss and FMR line-widths have been reported as low as 1 Oe for single crystal yttrium iron garnets [27]. With this wide range of possible materials, a criterion for choosing a material is needed. The criteria for choosing a material can be separated into three categories, FMR line-width, internal static field and saturation magnetization.

3.4.1 FMR Line-width

Without changing the resonance frequency, the FMR line-width (ΔH) has the greatest influence on the effectiveness of crosstalk reduction. Similar to ferrites used in microwave circuit elements such as isolators, circulators and filters, materials with narrow line-widths are needed. Although a broader line-width increases the width of the imaginary portion of the permeability spectrum over which resonance occurs the maximum value is drastically reduced. Thus the magnetic losses at resonance will not be nearly as strong. An example shown in Fig 3.6 shows the magnetic loss (μ'') for a line-width of 25 Oe and 50 Oe. The peak value of μ'' is approximately half when the line-width is increased from 25 Oe to 50 Oe. The broadening of the line-width is insignificant when compared to the change in peak value of μ''.

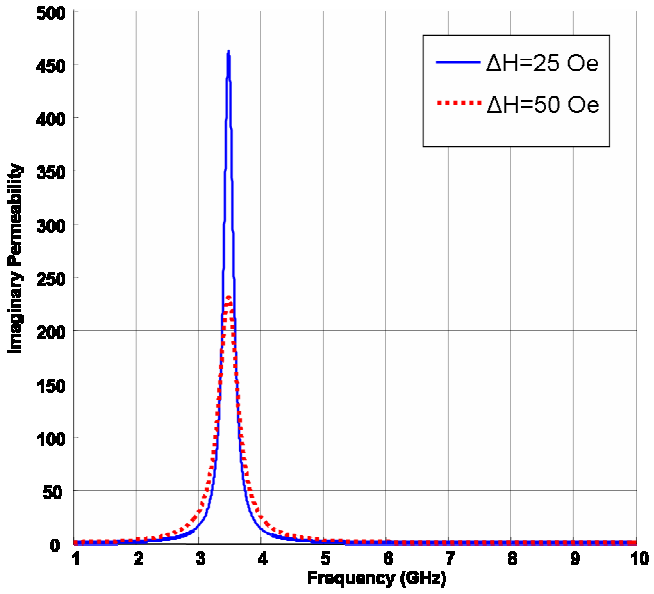

Fig. 3.6 The imaginary portion of the permeability spectrum demonstrating the effect of FMR line-width losses associated with FMR.

3.4.2 Internal Static Field

Internal static fields responsible for determining the frequency in which FMR will occure is dependent on any anisotropy fields and any externally applied fields if present. Ideally in this crosstalk suppression scheme, externally applied fields will not be needed as magneto crystalline anisotropy induced during fabrication will align the magnetic dipoles, alignment being held through shape anisotropy [34], [35]. Induced magneto crystalline fields up to 150 Oe have been reported for ferrites of similar dimensions used here [10]. This zero bias condition implies fields induced along the easy axis of magnetization as fields would have to be in excess of the magnitude of saturation magnetization in order to saturate along the hard axis [35]. Along with the induced fields, the shape anisotropy of the material must also be considered. This

shape anisotropy can have a large influence over what frequency FMR will occur. From (3.1)-(3.5), it can be seen that the dimensions of the ferrite are very influential on the resonance frequency along with saturation magnetization. Dimensions in which the thickness of the ferrite is much smaller than the width or the length dimensions of the ferrite, then the thickness will have the strongest effect. In general, a small internal magnetic field insuring saturation will result in the largest magnetic losses as the imaginary portion of the permeability will become larger [29].

3.4.3 Saturation Magnetization

The largest changes in FMR frequency are seen with changes in saturation magnetization ($4\pi M_s$). As with decreasing the internal static field, increasing the saturation magnetization will increase imaginary portion of the permeability and the magnetic losses will become greater [29]. Choosing a material with the highest saturation magnetization is desired for the best results.

3.5 Modeling Results

Similarly with the material characterization method demonstrated in chapter 2, 3D FEM electromagnetic simulation software (Ansoft HFSS 9.2) will be used to determine the scattering parameters of the coupled microstrips with and without the magnetic material. This allows for a wide range of material properties to be used as the crosstalk suppression material to be studied along with variations in material dimensions and placement.

3.5.1 Material Placement

As previously demonstrated by Kim *et al.* [10], placement of a ferromagnetic material on top of a coplanar waveguide has a significant effect on the insertion loss at resonance. This was also demonstrated by Bayard *et al.* [36] with the ferromagnetic material placed in the gap between the conductors of a coplanar waveguide. A similar increase in insertion loss occurs when a magnetic film is placed in the vicinity of a microstrip operating at the FMR frequency of the magnetic film. In the present application, the objective is to isolate circuit elements from one another without significantly affecting the insertion loss of the circuit itself. To avoid significant changes in the insertion loss, the magnetic film should be placed a sufficient distance away from any circuit element that is operating at the frequency in which FMR occurs in the magnetic film. Noting that the magnitude of the magnetic field is approximately inversely proportional to the distance from the microstrip, this distance can be relatively small. Achieving this can be done by either placing the magnetic film around one circuit element or between the circuit elements as shown in Fig. 3.7. The latter case is preferred as coupling primarily occurs at the substrate surface [37] and fabrication would not require additional steps in depositing an insulating layer to separate the ferrite from the conductor. Placement between circuit elements will be studied in terms of an offset distance (see Fig. 3.4) from the center of the space separating the two microstrips. The choice of placement for the magnetic film is determined by its magnetic properties as well as the circuit topology.

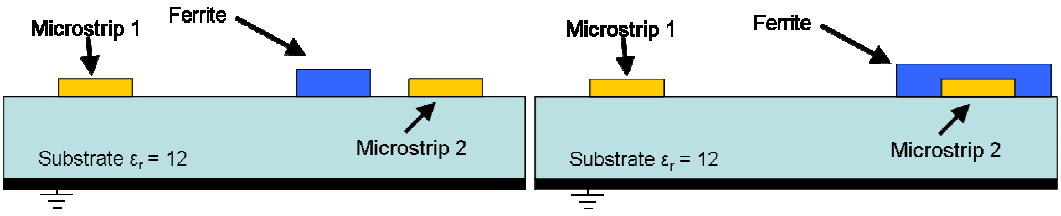

Fig. 3.7 Options for placement of magnetic film to suppress crosstalk. Topology on left of figure is preferred topology for the method discussed here.

As a first step in reducing the crosstalk between the microstrips, a magnetic film of width 100 μm, length 4 mm, and thickness 4 μm is placed symmetrically between the two microstrips. Material properties of the magnetic film are chosen initially to result in a resonance in the frequency band of 1 GHz to 10 GHz. With $4\pi M_s$ = 6000 Gauss, ΔH = 10 Oe, ε_r =10, μ_r =15 and internal magnetic field less shape anisotropy is 25 Oe. Shown in Fig. 3.8 and Fig. 3.9 the resulting S-parameters are obtained. A decrease in both the FEXT (S_{41}) and NEXT (S_{31}) can be seen at the FMR frequency of 3.8 GHz, accurately predicted by (3.1) – (3.5).

The improvement in both the NEXT and FEXT comes at a cost of an increase in insertion loss. Also the change in characteristic impedance caused by the addition of a magnetic film creates an unwanted change in the return loss. The resulting insertion loss and return loss with the addition of a magnetic film centered between the two microstrips is shown in Fig. 3.9.

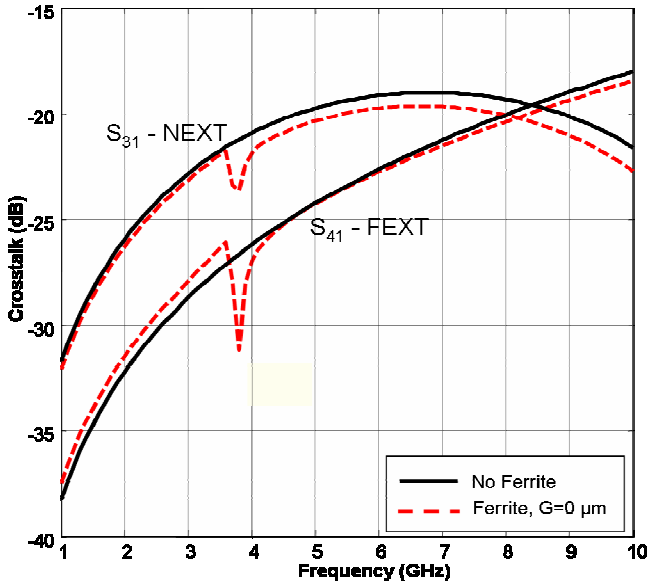

Fig. 3.8 NEXT and FEXT for a 4 mm long section of coupled microstrips with *i)* no magnetic film and *ii)* centered magnetic film (G = 0 μm), film thickness, t = 4 μm.

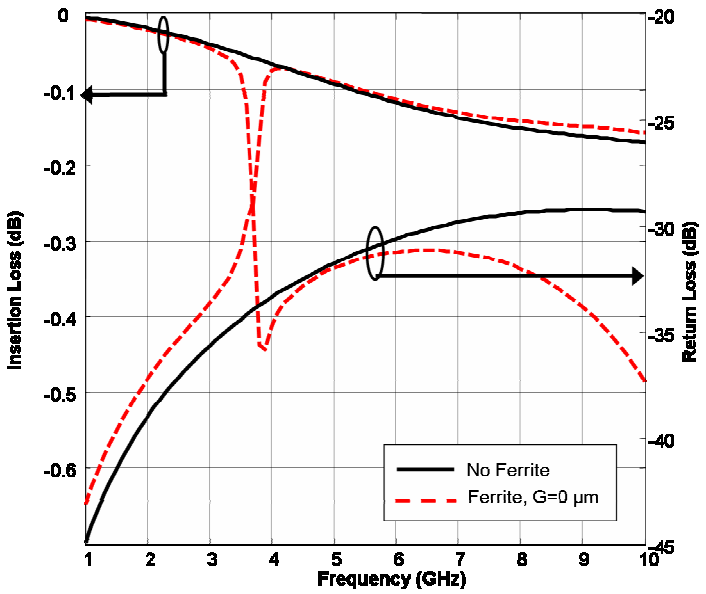

Fig. 3.9 IL (S_{21}) and RL (S_{11}) for a 4 mm long section of coupled microstrips with *i)* no magnetic film and *ii)* centered magnetic film (G = 0 μm), film thickness, t = 4 μm.

Changes in the return loss can easily be minimized with either the addition of a matching network or designing 50 Ohm microstrip with the magnetic material in proximity. Offsetting the magnetic film from the position in which it is centered between the microstrips can be used to improve the insertion loss of one of the microstrips. However it is important to note that although an offset will improve insertion loss in one of the microstrips, the reduction of crosstalk may either increase or decrease depending on factors to be discussed in section 3.5.3. In the case considered in this section a decrease in crosstalk is seen as the ferrite is offset from center.

Fig. 3.10 presents the near-end and the far-end crosstalk characteristics as a function of frequency for the structure with and without the magnetic film (t = 4 μm) for two cases of offset distance, G = 0 μm and G = 90 μm. For the offset magnetic film (G = 90 μm), it may be seen that there is an improvement in crosstalk reduction in the near-end (S_{31}) as well as the far-end (S_{41}) crosstalk at the resonant frequency compared with the magnetic film with no offset (G = 0 μm). Both offset cases are accurately predicted to be at 3.8 GHz using (3.1)-(3.5). For an offset of 90 μm, the crosstalk suppression improved from -28dB to -33 dB. Fig. 3.11 shows the insertion loss, S_{21} and the return loss, S_{11} in dB for the same configuration. The insertion loss indicates an increase of the order of -0.28 dB for the centered magnetic film, and nearly an improvement by one half to -0.15 dB for the 90 μm offset compared to the case with no magnetic film. There was a slight deterioration in the return loss at resonance for the centered case. However, the offset case shows an improvement.

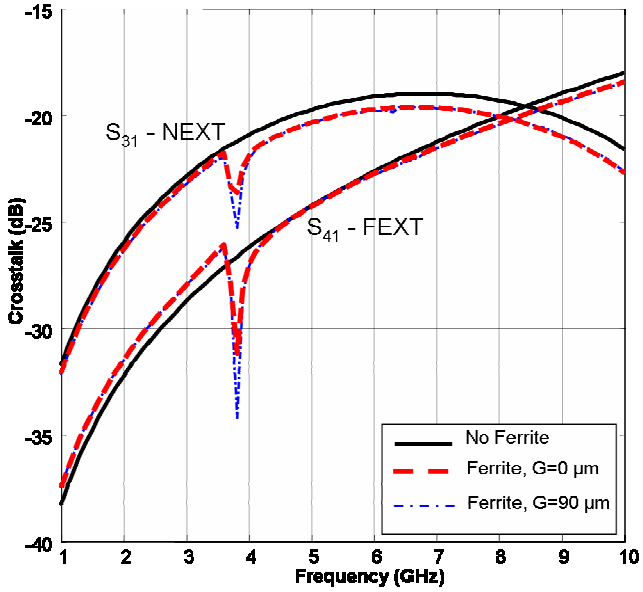

Fig. 3.10 Near-end and far-end crosstalk for a 4 mm long section of coupled microstrips with *i)* no magnetic film *ii)* centered magnetic film and *iii)* offset magnetic film (G = 90 µm), film thickness, t = 4 µm.

Fig. 3.12 shows the comparison between the insertion losses for the microstrip conductors 1 and 2 (S_{21} and S_{43}, respectively) for the offset of 90 µm. An increase in the insertion loss, S_{43}, at the resonant frequency for the second microstrip is expected. This is due to the fact that when the distance between one microstrip and the magnetic material is increased, it will now be closer to the other microstrip. The insertion loss, S_{43} will not be affecting the performance of the second microstrip as long as it is intended to operate at any frequency other than the resonant frequency.

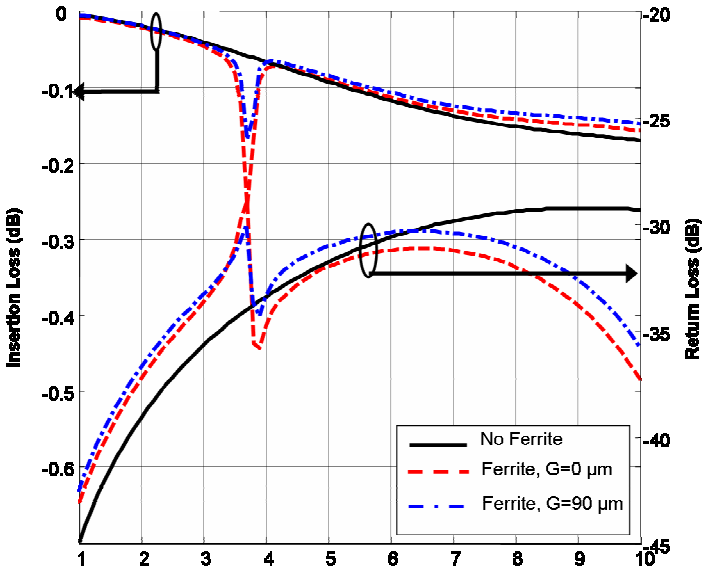

Fig. 3.11 Insertion loss and return loss for a 4 mm long section of coupled microstrips with *i)* no magnetic film *ii)* centered magnetic film and *iii)* offset magnetic film (G = 90 µm), film thickness, t= 4 µm.

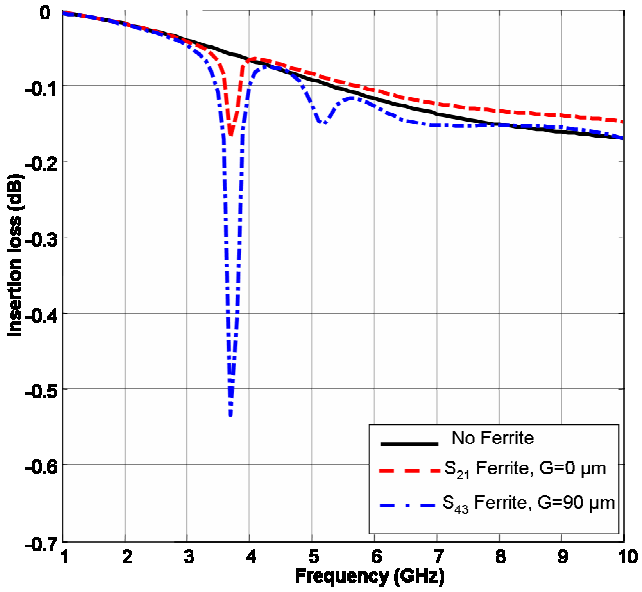

Fig. 3.12. Insertion loss for 4 mm long section of coupled microstrips. Magnetic material offset by 90 µm and a thickness of 4 µm.

With sufficient spacing between the microstrip and the magnetic film, insertion losses for the microstrip can be made negligible at resonance. Most important is the fact that at off resonance, the magnetic material has very little to no effect on any of the scattering parameters.

The proposed topology has many applications in mixed signal circuits. For instance, a supply line operating at low frequencies or DC can be isolated from a high speed circuit element by placing a magnetic film closer to the supply line as shown in Fig. 3.13. This effect can also be obtained in cases where two high frequency lines operating at different frequencies are kept at close proximity. Examples include RF, LO and IF signals in the case of a mixer. The magnetic film should have a resonance frequency that corresponds to the frequency of the circuit element at which the isolation is required.

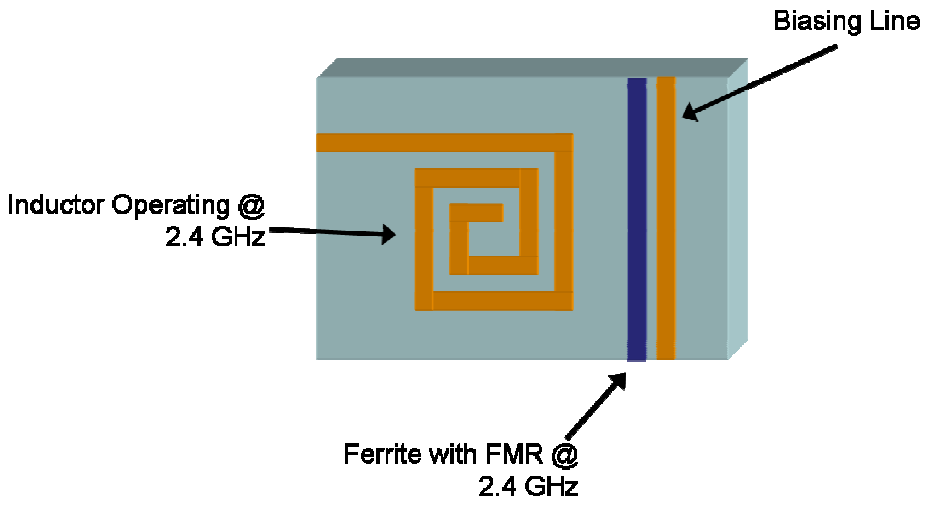

Fig. 3.13 An example of how a magnetic film should be placed closer to one circuit element than the other in order to have minimum effect on IL of the inductor and maximum isolation from the biasing line.

3.5.2 Effect of FMR Line-width

As previously mentioned, FMR line-width plays one of the most important roles in determining how effective crosstalk will be suppressed. With narrower line-widths providing the most isolation, materials such as Yttrium Iron Garnets (YIG) or Calcium – Vanadium substituted YIG would be ideal candidates in this application. Typically used in high performance circulators and isolators, these materials possess the narrowest of line-widths. Shown in Fig. 3.14, three variation of FMR line-width are shown and the resulting effect on the far-end crosstalk (S_{41}). As it can be seen the narrow line-width of 10 Oe shows the greatest suppression of crosstalk. This is in agreement with Stoner-Wolfwarth, stating that narrower line-widths will produce a higher peak value at resonance in the dissipative portion of the permeability (μ'') [29].

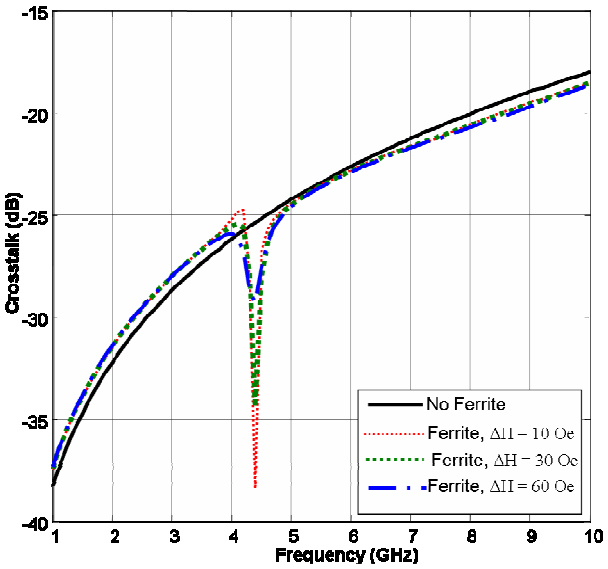

Fig. 3.14 Effect of FMR line-width on FEXT (S_{41}) for material properties 6000 Gauss, $\varepsilon_r = 10$, $\mu_r = 15$ and physical properties of $L = 4$ mm, $G = 75$ µm, $W = 100$ µm and $t = 6$ µm.

3.5.3 Effect of Internal Static Field

The resonant frequency at which the magnetic film can be useful in crosstalk suppression is governed by (3.1), which is dependent on both the physical dimensions and the material properties of the magnetic material. For a given set of physical dimensions and material characteristics, the resonant frequency can be varied by changing the thickness of the magnetic material. Fig. 3.15 shows the far-end crosstalk for five different t values and G = 0 μm. It may be seen that the resonant frequencies obtained from the full-wave simulations for these three cases are 3.8 GHz, 4.1 GHz, 4.7 GHz, 4.8 GHz and 4.9 GHz compared to the theoretically predicted values of 3.9 GHz, 4.33 GHz, 4.71 GHz, 5.07 GHz and 5.40 GHz respectively. As it is seen, accuracy between predicted and simulated resonance is decreasing as thickness is increased. This could be in part due to the assumption made in (3.3) and (3.4) for which demagnetizing factors are based only on approximations for a rectangular shape. Also noticeable is the improvement in crosstalk as thickness in increased, but it appears there is a value in which crosstalk suppression is at a maximum, after which the benefits decrease. For this circuit topology, 6 μm has the greatest effect on both the near-end and far-end crosstalk. For a thickness of 6 μm, the crosstalk is improved by 16.5 dB and 6.5 dB for the far-end and near-end respectively. Referring to equations (3.1)-(3.5), it may be noticed that since $L>>t$, changing the length from 4 mm to other values (higher or lower, provided it is sufficiently larger than t) will not alter the resonant frequency significantly. This is one of the main advantages of this

scheme, since the resonant frequency is nearly independent of the length under consideration.

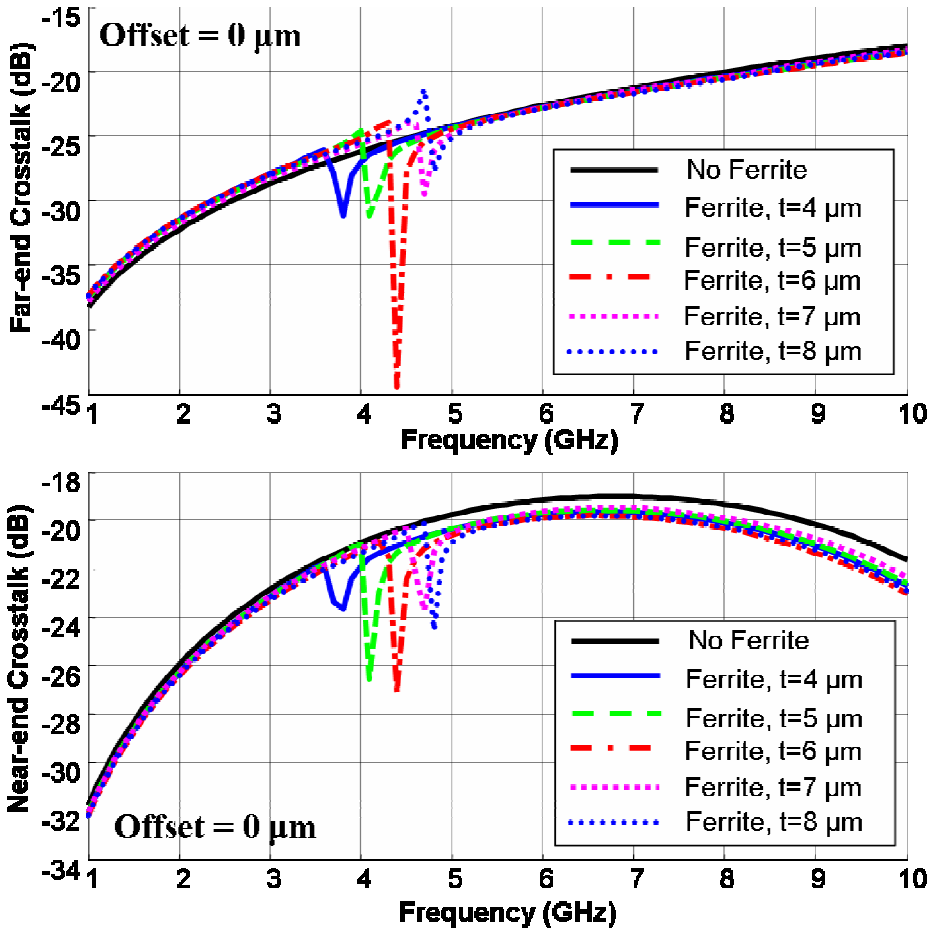

Fig. 3.15 Far-end and near-end crosstalk for 4 mm long section of coupled microstrips shown with an increase in the thickness of the magnetic film centered at $G = 0$ µm.

As suggested in section 3.5.1, an offset may be used to lessen any negative effects, such as increased insertion or return losses. In the case of a film with a thickness equal to 4 µm, a ferrite offset of 90 µm shows an improvement in both the near-end and far-end crosstalk over a centered ferrite (see Fig. 3.10). A similar

statement made concerning the ferrite offset and improvements in insertion and return loss cannot be made regarding ferrite offset and crosstalk reduction. As seen in Fig. 3.16, as the thickness of the ferrite is increased, with $G = 90$ μm, the effect on the far-end crosstalk is reduced and the near-end crosstalk shows a similar trend to that of the centered ferrite. With the ferrite offset by 90 μm, it would appear that if the desired effect were to isolate the far-end port, a 4 μm film would be ideal, whereas if the near-end was more essential to isolate, a 7 μm film would be chosen. If it is desired to achieve maximum reduction in crosstalk in the total system, both near-end and far-end, total coupled power absorbed should be observed.

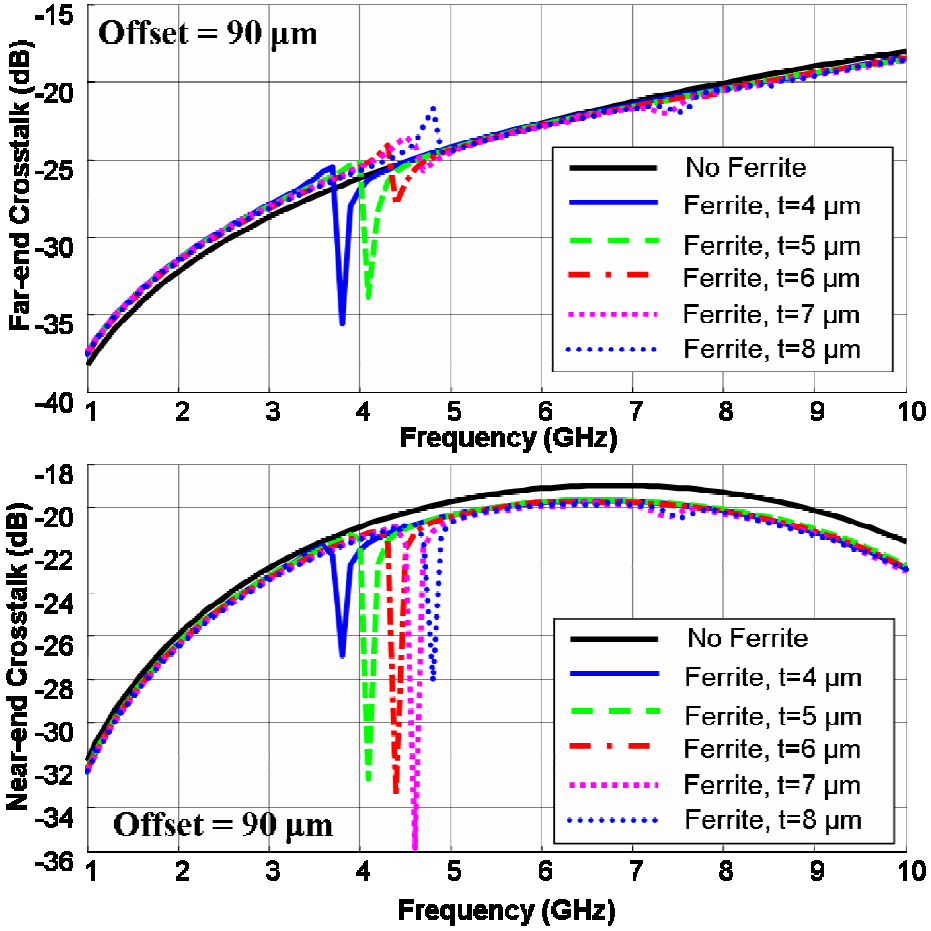

Fig. 3.16 Far-end and near-end crosstalk for 4 mm long section of coupled microstrips shown with an increase in the thickness of the magnetic film offset at G = 90 µm.

3.5.4 Power Absorption

A way to look at the maximum crosstalk suppression is in terms of the total power coupled to the near-end and the far-end ports. Let P_w and P_{wo} be defined as the total crosstalk power with and without the magnetic film as shown in (3.6)-(3.7). We define crosstalk coefficient C_m as the ratio of the two crosstalk powers as shown in (3.8).

$$P_{wo} = \left|S_{31wo}\right|^2 + \left|S_{41wo}\right|^2 \tag{3.6}$$

$$P_{w} = \left|S_{31w}\right|^2 + \left|S_{41w}\right|^2 \tag{3.7}$$

$$C_m = \left(\frac{P_w}{P_{wo}}\right) dB \tag{3.8}$$

Fig. 3.17 shows the crosstalk coefficient, C_m as a function of frequency for five different film thicknesses centered between the microstrips. It can be seen that at off resonance, the crosstalk coefficient is nearly equal to 0 dB indicating that the magnetic film has little influence on the transmission properties. However, at resonance, the effect of crosstalk suppression is evident for all five cases. As expected from examination of Fig. 3.15, the case with t = 6 μm and G = 0 μm allows for the greatest crosstalk suppression at nearly -8 dB. This indicates that the total coupled power with the 6 μm magnetic film is reduced by 83% compared to the case with no magnetic film, which is considered as a significant improvement.

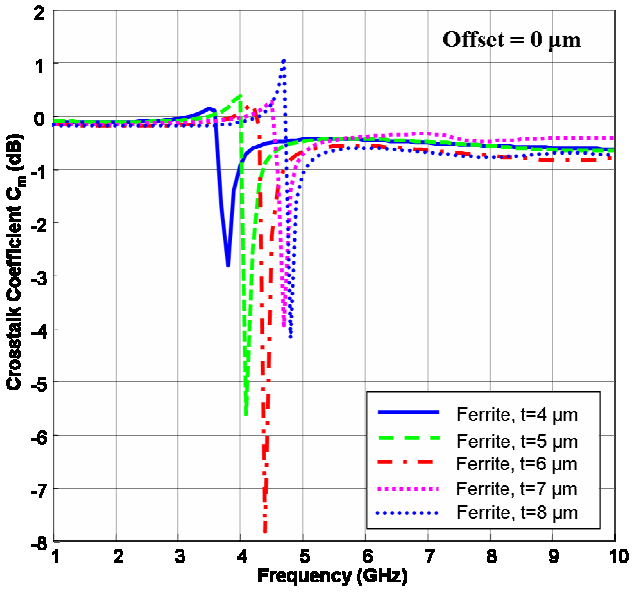

Fig. 3.17 Variation of Crosstalk Coefficient, C_m as a function of frequency for different magnetic film thicknesses with the magnetic film centered at $G = 0$ µm.

Determining the optimum film thickness and placement is not always as apparent from inspection of the far-end and near-end response, such as the case when the magnetic film was centered between the microstrips. In the case of the offset G = 90 µm, it is clearly seen from Fig. 3.16 that with increased film thickness, crosstalk suppression on the far-end is reduced and near-end suppression sees a maximum at 7 µm. By examining the total power of both the near-end and far-end we can see in Fig. 3.18 that a total suppression of -10.55 dB, or 91% reduction, occurs with a film thickness of 5 µm.

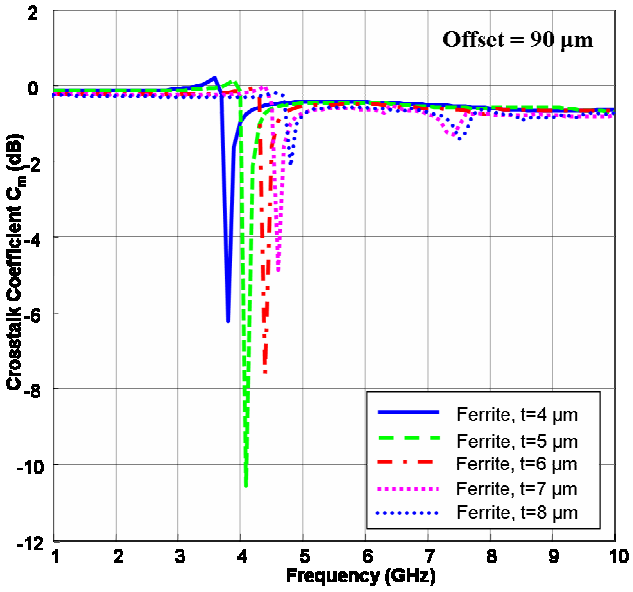

Fig. 3.18 Variation of Crosstalk Coefficient, C_m as a function of frequency for different magnetic film thicknesses with the magnetic film offset at G = 90 µm.

Possibly of more importance to design engineers is the amount of space reduction using this film could result in. A comparison can be made to see how this magnetic film can significantly reduce spacing between components. A similar microstrip structure as shown in Fig. 3.1 with the spacing between microstrips increased from 300 µm to 725 µm results in a near-end crosstalk of -32.6 dB and far-end crosstalk of -34 dB at 4.1 GHz. Comparing this with the 5 µm film shown in Fig. 3.16, it can be seen that at resonance the near-end and far-end crosstalk both match with the amount of crosstalk for the microstrips spaced 725 µm apart with no magnetic film. This correspond to the microstrips only needing to be separated apart from each other by 41% of the original space needed.

3.5.5 Effect of Saturation Magnetization

Similar to the dimensional effects associated with FMR, saturation magnetization of the magnetic film will also have very strong influence over the resonant frequency, where suppression can occur. Fig. 3.19 shows the effect of varying the saturation magnetization of material on the resonant frequency. An internal field of 25 Oe and dimensions of the magnetic film (thickness of 4 μm and width of 100 μm) are kept the same as for the previous cases. It may be noticed that the resonance frequency can be tuned to be anywhere in the frequency band between 2 GHz and 5 GHz by varying the saturation magnetization from 4 kGauss to 8 kGauss. Table 3.1 shows the predicted values of resonant frequency computed using (3.1)-(3.5) versus the values obtained from the full-wave electromagnetic simulation response. The percentage deviation for each case is also indicated in the table. It may be seen that for all values of saturation magnetization, the resonant frequency matches closely with the predicted values.

Table 3.1 Resonant Frequency versus Saturation Magnetization

$4\pi M_s$ (Gauss)	Full-Wave Simulation Resonant Freq. (GHz)	Predicted Resonant Freq. (GHz)	% Error
4000	2.6	2.65	1.89
5000	3.2	3.27	2.14
6000	3.8	3.90	2.56
8000	4.97	5.14	3.31

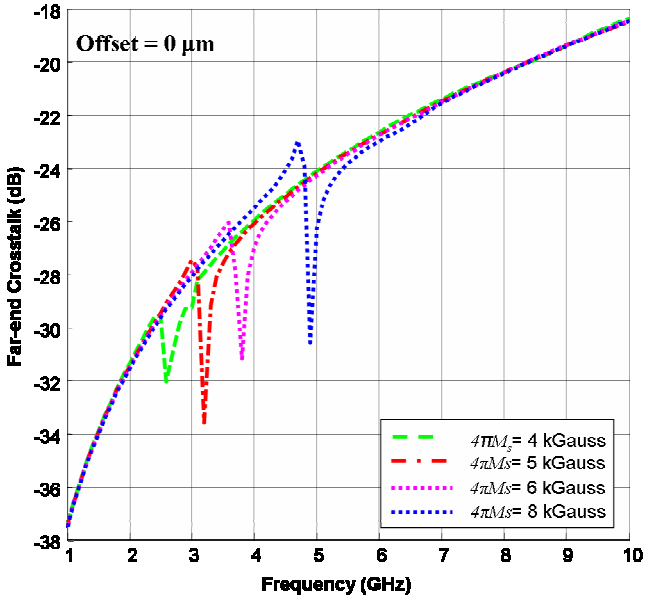

Fig. 3.19 Far-end crosstalk for 4 mm long section of coupled microstrips. Magnetic material centered and thickness of 4 µm with a variation in saturation magnetization ($4\pi M_s$).

4 Crosstalk Suppression – Measurement Results

4.1 Experimental Setup

A test structure similar to that described in chapter 3 is fabricated on Rogers Corp. RT/Duroid® 5880 substrate ($\varepsilon_r = 2.2$ $\mu_r = 1$, $tan\delta_e = .0004$, substrate height = 31 mil) and is shown in Fig. 4.1 with ferrite film deposited. Two 50 ohm microstrip lines, with a width of 2.38 mm and spacing of s = 2mm, are fabricated. Ninety degree flares are used to accommodate SMA connectors and provide sufficient isolation between terminals. Frequency dependent S-parameter data is measured using a Hewlett Packard 5722C vector network analyzer (VNA). Calibration using the standard SOLT (short-open-line-through) method is used to shift the reference plane to the 3.5 mm SMA connectors used to interface between the device and the VNA.

4.2 Materials

As previously discussed materials possessing high saturation magnetization and narrow line-widths are needed for this method of crosstalk suppression. Two materials with these characteristic obtained from Trans-Tech, Inc., YIG (G-1210) and Calcium – Vanadium substituted YIG (TTVG-1850). Both materials come standard in disk form which can be prepared to be deposited in our application. G-1210 material properties are: $4\pi M_s$ = 1200 Gauss, ΔH = 30 Oe, ε_r = 14.8, μ_{intial} = 87, $tan\delta_e$ = .0002, Br = 784 Gauss and H_c = 0.69 Oe. Where μ_{intial} is initial permeability, B_r is remanent induction and H_c is coercive force. TTVG-1850 material properties are:

$4\pi M_s$ = 1850 Gauss, ΔH = 7 Oe, ε_r = 15, μ_{intial} = 380, $tan\delta_e$ = .0002, Br = 1280 Gauss and H_c = 0.5 Oe.

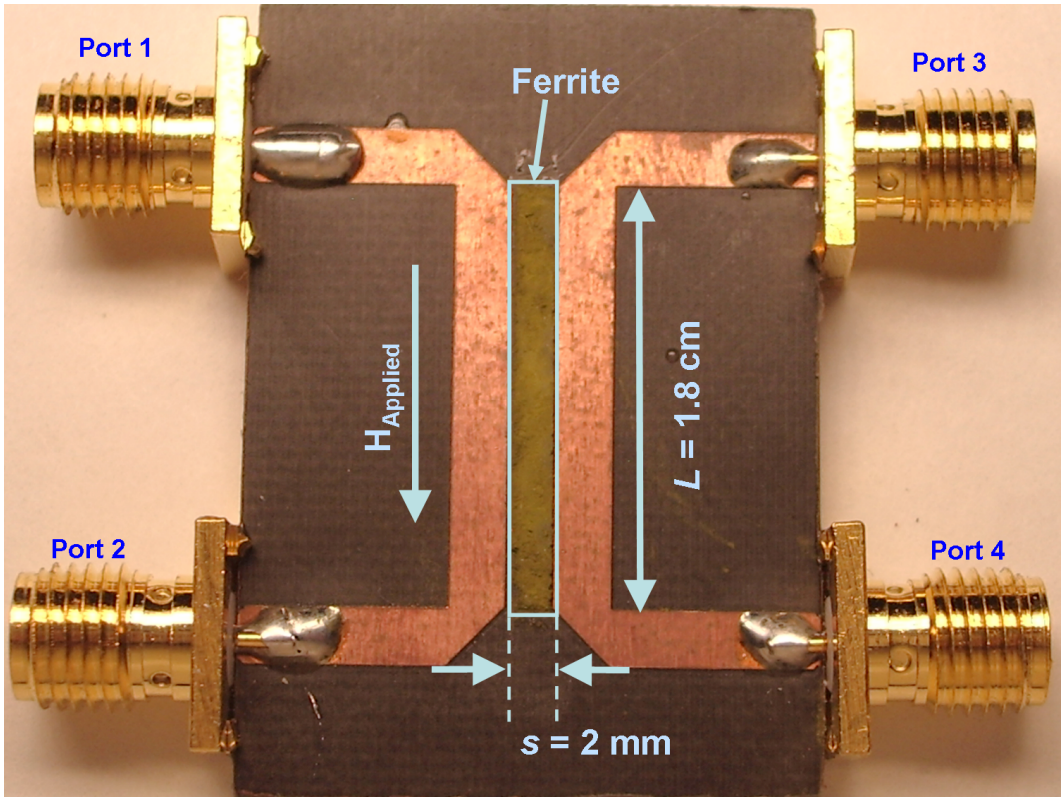

Fig. 4.1. Test structure fabricated on RT/Duroid® 5880 substrate with ferrite film deposited between microstrip conductors.

4.3 Film Preparation

Using a vibratory mill, individual disks of each material are ground for 4 hours to produce a fine powder. Combining this powder with an adhesive, the paste is applied into rectangular patches between the microstrips using a mask as shown in Fig. 4.1 and allowed to dry for several hours. This method will inevitably result in a

film with a much broader line-width compared to that of the disk obtained from Trans-Tech, Inc. Porosity, significant in line-width broadening [38], can be reduced through compression as film is drying but still can be expected to be much greater than when in disk form. The resulting film is shown in Fig. 4.1 for the G-1210 material. Controlling the physical dimensions of width and length of the magnetic material is limited to accuracy of the mask placement. Film thickness is not accurately controlled and is a major limiting factor when using this method of film preparation.

4.4 Measurements

The method of film preparation used here does not allow for an induced remnant field to be established in the film needed for a zero biasing condition. Alternatively, an external biasing source can be used to set up a static magnetic field within the film. This external biasing source is realized in the form of a solenoid. The solenoid built applies a magnetic field in the direction shown in Fig. 4.1. Fields ranging from $H_{applied}$ = 0 Oe to $H_{applied}$ = 130 Oe are obtainable with over 90% uniformity over the entire length of the magnetic film.

4.4.1 Yttrium Iron Garnet: G-1210

The first film tested is the YIG film with material properties $4\pi M_s \approx 1200$ Gauss, $\Delta H \geq 30$ Oe, $\varepsilon_r \approx 14.8$, $\mu_{intial} \approx 87$, $tan\delta_e \approx .0002$, $Br \approx 784$ Gauss and $H_c \approx 0.69$ Oe. The film was prepared to be centered between the microstrips with t = 225 μm, W = 1.9 mm and L = 1.8 cm. The surface roughness is significant enough to be seen

with the unaided eye. Shown in Fig. 4.2 the resulting far-end and near-end crosstalk for an applied bias of $H_{applied}$ = 130 Oe. This case shows a 20 dB improvement in the far-end crosstalk compared to the direction coupler with no magnetic material. A reduction in the crosstalk is also seen in the near-end of the directional coupler with a change from -29 dB to -30 dB. Although the most dramatic effect is seen in the far-end crosstalk, near-end crosstalk suppression would be more apparent with increased lengths of coupled microstrips and magnetic film. Applying the dimensions and magnetic properties of the material to (3.1), a resonance is predicted to occur at 1.7 GHz. The resonance seen in Fig. 4.2 occurs at 1.5 GHz, this discrepancy is most likely due to changes in the magnetic properties of the film incurred during fabrication and the significant surface roughness seen in the film.

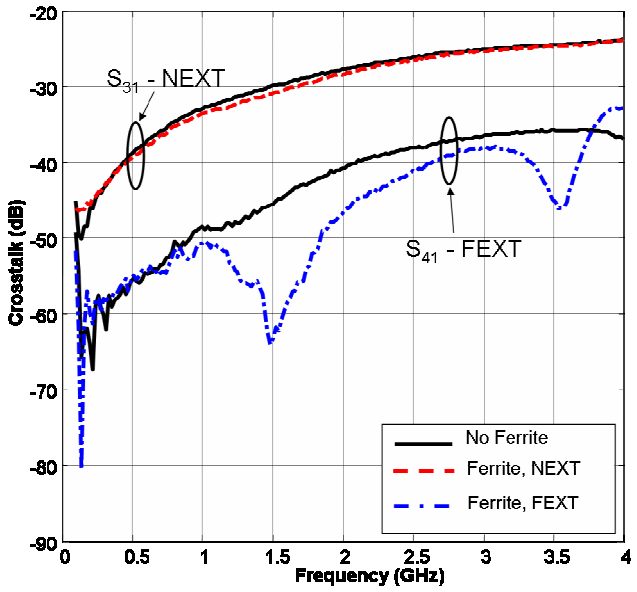

Fig. 4.2 Near-end and far-end crosstalk for the fabricated test structure with no magnetic film and with YIG: G-1210 magnetic film acting as a crosstalk suppressor.

Network analyzer resolution prevents study of changes in insertion losses, expected to be of the order of a few tenths of a dB. Total coupled power absorbed, as described in chapter 3, is shown in Fig. 4.3. The overall effectiveness of this magnetic film on crosstalk suppression can be seen in the crosstalk coefficient, C_m, to be over 1 dB in power reduction, corresponding to approximately a suppression of crosstalk by over 20 %.

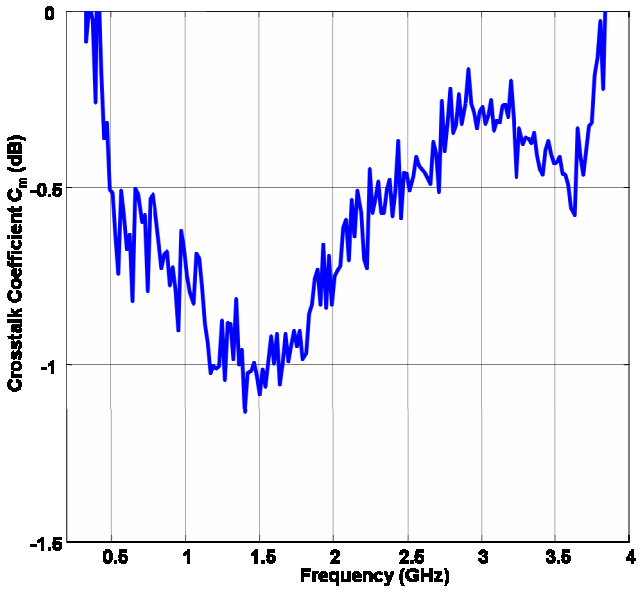

Fig. 4.3 Crosstalk Coefficient, C_m as a function of frequency with YIG: G-1210 magnetic film acting as a crosstalk suppressor.

4.4.2 Calcium – Vanadium Substituted Yttrium Iron Garnet: TTVG-1850

The second film tested is prepared from calcium – vanadium substituted YIG (CV-YIG) with material properties $4\pi M_s \approx 1850$ Gauss, $\Delta H \geq 7$ Oe, $\varepsilon_r \approx 15$, $\mu_{intial} \approx 380$, $tan\delta_e \approx .0002$, $Br \approx 1280$ Gauss and $H_c \approx 0.5$ Oe. The film is centered between

the microstrips and has a thickness, t = 200 μm, W = 1.9 mm and L = 1.8 cm. This material having a much narrower line-width than the previous material, it is expected to result in a more significant reduction in crosstalk at resonance. Shown in Fig. 4.4 the near-end and far-end crosstalk response for the TTVG-1850 film is plotted with applied bias of $H_{applied}$ = 130 Oe, along with the response when no magnetic film is present. A significant decrease in crosstalk at resonance in the far-end is seen with the CV-YIG film, providing isolation from -38 dB to nearly -70 dB. This level of isolation would be very desirable in many applications that are highly sensitive to noise. Also an improvement in the near-end crosstalk is seen of a few dB at resonance. Using (3.1) the resonant frequency, measured at 2.27 GHz is very accurately predicted to be 2.32 GHz.

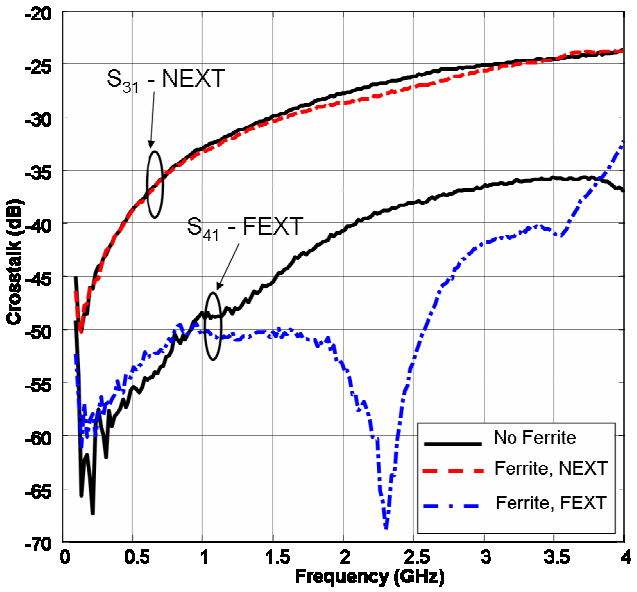

Fig. 4.4 Near-end and far-end crosstalk for the fabricated test structure with no magnetic film and with CV-YIG: TTVG-1850 magnetic film.

Again the VNA is insensitive to the small variations in insertion losses. Observing the coupled power absorbed, it can be seen that the crosstalk coefficient has increased from approximately -1 dB to -1.5 dB when compared with the YIG: G-1210. This effectively corresponds to a total reduction in crosstalk of nearly 30%. Although not as significant of a reduction as predicted in simulation, further advances in the fabrication techniques could allow films to be produced much thinner and more uniform, allowing these goals could be reached.

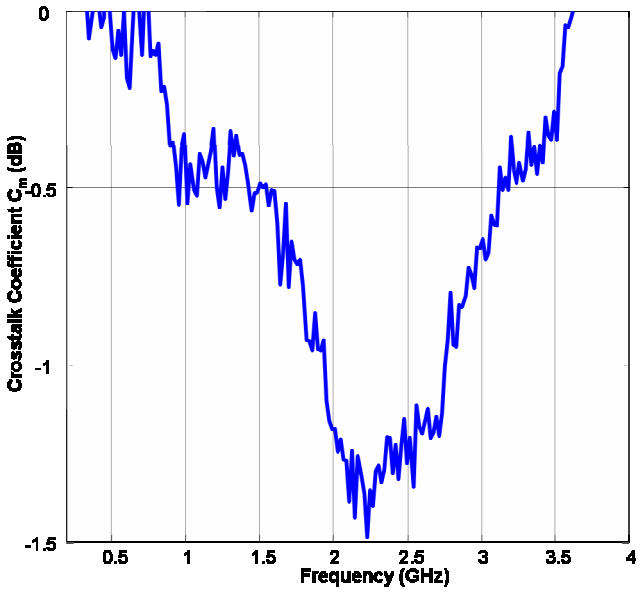

Fig. 4.5 Crosstalk Coefficient, C_m as a function of frequency with CV-YIG: TTVG-1850 magnetic film acting as a crosstalk suppressor.

5 Conclusion and Future Work

5.1 Conclusion

A purposed method for fast characterization of magnetic materials over microwave frequencies is shown in this thesis. This method is validated using 3D EM simulations and an accuracy of nearly 98% is shown for the extraction of permittivity, permeability, saturation magnetization and FMR line-width. The ability to simultaneously extract several material properties over broadband frequencies using equipment readily available in most laboratories proves this method to be highly desirable to be used in conjunction with the crosstalk suppression scheme presented here.

The study of a novel means for crosstalk suppression using magnetic films is the primary focus of this thesis. Using 3D EM simulations, a study of closely coupled microstrip interconnects is performed by placing a magnetic film in the space separating to adjacent microstrips, similar to the implementation of a guard trace. A thorough investigation is carried out to evaluate the effect of the material properties as well as the physical dimensions of the magnetic film for effective crosstalk suppression. It is shown that the magnetic film will inherently change the insertion loss as well as the return loss of the circuit. This effect is shown to be minimized when using the magnetic film to isolate components running at different operating frequencies, such as a bias line isolated from a high frequency component. Comparing the amount of crosstalk reduced over several thicknesses, it can be seen

that a depending on the offset of the magnetic material, there could be an optimum thickness that results in maximum crosstalk reduction. Using the case of $4\pi M_s$ = 6000 Gauss, ΔH = 10 Oe and an offset of 90 μm, it is seen that the optimum film thickness is 5 μm. This thickness and offset results in a total reduction of crosstalk of over 90%. In terms of component spacing, the amount of crosstalk resulting from two microstrips spaced 725 μm apart without any magnetic film would be equivalent to the amount of crosstalk seen at resonance in the microstrips spaced 300 μm apart with a magnetic film. This is equal to a reduction in space by nearly 60% of the original size and resulting in the equal amount of isolation between circuit elements.

As verification of the 3D EM simulations, microstrip directional couplers are fabricated on an RT/Duroid® substrate. Two magnetic films are prepared using ferrite disks and the films are applied to the microstrip directional coupler. The first set of YIG films demonstrate a definite resonance point that is fairly accurately predicted using Kittel's condition for resonance. Although there is not a significant change in near-end crosstalk, far-end crosstalk is isolated to beyond -60 dB. A total reduction of crosstalk is seen at approximately 20% and with further control over film dimensions, this number could most likely be reduced even further. The second film, CV-YIG, results in even greater crosstalk suppression at over 30%, with far-end reduction of nearly -70 dB. With better film preparation, allowing for thinner and more uniform films, an improvement from the results demonstrated here is expected.

5.2 Future Work

Future work to be considered in the area of material characterization would first be in the area of fabrication. Although the planar structure is must easier to fabricate than a method based on a coaxial platform, a method for fabrication still needs to be developed. Also, a method to extract the off-diagonal components of the permeability tensor could be developed. The issue of inaccurate results occurring in measurement of low-loss materials [16] could also be addressed.

Much work to be done in the crosstalk suppression method presented here is in the development of an optimization scheme in which the best material dimensions and placement could be determined given the circuit topology and magnetic material properties. Another important area yet to be explored is the possibility of increasing the bandwidth of operation. This could possibly be achieved by using several magnetic materials with different FMR frequencies. The superposition of the crosstalk suppression provided by each film could result in an increase in bandwidth. An area that would prove to be highly desirable in crosstalk suppression, but would also have many other uses would be the ability to tune the FMR frequency over a large frequency band. Achieving this with some type of latching structure, that could easily bias the ferrite in circuit would allow for the FMR frequency to be controlled.

Besides the application of this topology as a method to suppress crosstalk, there could be several applications as a separate circuit element all in itself. Such as being implemented as a notch filter, isolator, or even a directional coupler with further directional control not obtainable with standard designs.

Bibliography

[1] L. Green, *Circuits and Devices Magazine*, IEEE vol. 15, Issue 6, pp. 7– 10, Nov. 1999.

[2] D. G. Kam, H. Lee, J. Kim, J. Kim, *Microwave and Wireless Components Letters*, IEEE vol. 13, Issue 9, pp. 411 – 413, Sept. 2003.

[3] G. Ponchak et. al., "The Use of Metal Filled Via Holes for Improving Isolation in LTCC RF and Wireless Multichip Packages," *IEEE Trans. Advanced Packaging*, Feb. 2000.

[4] M. Kim, "Crosstalk control for microstrip circuits on PCBs at microwave frequencies," *Electromagnetic Compatibility, IEEE International Symposium on*, Aug. 1995 pp. 459-464.

[5] J. Gipprich, D. Stevens, "A new via fence structure for crosstalk reduction in high density stripline packages," *Microwave Symposium Digest*, 2001 IEEE MTT-S International, Vol.3, 2001, pp. 1719-1722.

[6] J.P.K. Gilb, C. A. Balanis, "Coupling reduction in high-speed, high-density digital interconnects with substrate compensation," *Electrical Performance of Electronic Packaging*, April 1992 pp. 116 – 118.

[7] K. H. Kim, S. Ikeda, M. Yamaguchi, K. Arai, "FEM analysis on the effects of soft magnetic film as a noise suppressor at GHz range," *Journal of Applied Physics*, vol. 93, No. 10, pp. 8588-8590, May 2003.

[8] S. Ohnuma, H. Nagura, H. Fujimori, and T. Masumoto, "Noise Suppression Effect of Nanogranular Co Based Magnetic Thin Films at Gigahertz Frequency," *IEEE Trans. On Magnetics*, vol. 40, pp. 2712-2715, July 2004.

[9] M. Yamaguchi, K. H. Kim, T. Kuribara, and K. Arai, "Thin-Film RF Noise Suppressor Integrated in a Transmission Line," *IEEE Trans. On Magnetics*, vol. 38, No. 5, pp. 3183-3185, Sept. 2002.

[10] K. H. Kim, S. Bae, and M. Yamaguchi, "Dimensional Effects of the Magnetic Film on Coplanar Transmission Line for RF Noise Suppression," *IEEE Trans. On Magnetics*, vol. 40, pp. 2847-2849, July 2004.

[11] H. Ono, T. Ito, S. Yoshida, Y. Takase, O. Hashimoto, and Y. Shimada, "Noble Magnetic Films for Effective Electromagnetic Noise Absorption in the

Gigahertz Frequency Range," IEEE *Trans. On Magnetics*, vol. 40, pp. 2853-2857, July 2004.

[12] K. H. Kim, M. Yamaguchi, S. Ikeda, K. Arai, "Modeling for RF Noise Suppressor Using a Magnetic Film on Coplanar Transmission Line," *IEEE Trans. On Magnetics*, vol. 39, pp 3031-3033, Sept 2003.

[13] K. Kim, S. Ohnuma, M. Yamaguchi,, "RF Integrated Noise Suppressor Using Soft Magnetic Films," *IEEE Trans. On Magnetics*, vol. 40, pp. 2838-2840, July 2004.

[14] S. K. Koul, B. Bhat, *Microwave and Millimeter Wave Phase Shifters, Volume I: Dielectric and Ferrite Phase Shifters*, 1991, Artech House, Boston.

[15] J. Hu A. Sligar, C. Chang, S. Lu R. K. Settaluri, "A grounded coplanar waveguide technique for microwave measurement of complex permittivity and permeability," *IEEE Trans. On Magnetics*, vol. 42, pp. 1929 - 1931, July 2006.

[16] J. Hinojosa, "S-Parameter Broadband Measurements On-Coplanar and Fast Extraction of the Substrate Intrinsic Properties," *IEEE Microwave Wireless Compon. Lett.*, vol. 11, No. 2, Feb. 2001.

[17] J. Hinojosa, "S-Parameter Broad-Band Measurements On-Microstrip and Fast Extraction of the Substrate Intrinsic Properties," *IEEE Microwave Wireless Components Letters*, vol. 11, No. 7, July 2001.

[18] W. B. Weir, "Automatic measurement of complex dielectric constant and permeability at microwave frequencies," *Proc. IEEE,* vol. 62, no. 1, pp. 33-36, Jan. 1974.

[19] D. Vincent, T. Rouiller, C. Simovsky, B. Bayard, G. Noyel, "A new Broad-Band Method for Magnetic Thin-Film Characterization in the Microwave Range," *IEEE Trans. Microwave Theory Tech.*, vol. 53, No. 4, April 2005.

[20] B. Kang, J. Cho, C. Cheon, Y. Kwon, "Nondestructive Measurement of Complex Permittivity and Permeability Using Multilayered Coplanar Waveguide Structures," *IEEE Microwave Wireless Compon. Lett*., vol. 15, no. 5, May 2005.

[21] G. Counil, K. Joo-Von, T. Devolder, C. Chappert, K. Shigeto, and Y. Otani, "Spin wave contributions to the high-frequency magnetic response of thin films obtained with inductive methods,", *J. Appl.Phys*.. 95, pp. 5646-5652, May 2004.

[22] M. L. Schneider, A. B. Kos, and T. J. Silva, "Finite coplanar waveguide width effects in pulsed inductive microwave magnetometry," *Appl. Phys. Lett*. 85, pp. 254-256, July 2004.

[23] G. L. Mattahei, K. Kiziloglu, N. Dagli, S. I. Long, "The Nature of the charges, Currents, and Fields in and About Conductors Having Cross-Sectional Dimensions of the Order of a Skin Depth," *IEEE Trans. Microwave Theory Tech*., vol. 38, No. 8, Aug. 1990.

[24] E. Carlsson, S. Gevogrian, "Conformal Mapping of the Field and Charge Distributions in Multilayered Substrate CPW's," IEEE *Trans. Microwave Theory Tech*., vol. 47, No. 8, Aug. 1999.

[25] D. M, Pozar, Microwave *Engineering*, Addison-Wesley, 1990.

[26] C. Kittel, "On the Theory of Ferromagnetic Resonance Absorption," *Physical Review*, vol. 73, pp 155-161, Jan. 1948.

[27] B. Lax, K. J. Button, Microwave *Ferromagnetic materials and Ferrimagnetics*. McGraw-Hill, 1962.

[28] D. Spenato, A. Fessant, J. Gieraltowski, J. Loaec, H. Le Gall, "Theoretical and experimental approach of spin dynamics in in-plane anisotropic amorphous ferromagnetic thin films," *J. Phys. D,* 26, pp. 1736-1740, (1993).

[29] E. C. Stoner, E. P. Wohlfarth, *Trans. Roy. Soc*. A240, 599 (1948).

[30] A. G. Gurevich, *Ferrites at microwave frequencies*, 1961, Consultants Bureau

[31] G. Bertotti, A. Magni, I. D. Mayergoyz, C. Serpico, "Landau-Lifshitz magnetization dynamics and eddy currents in metallic thin films," *Journal of Applied Physics*, vol. 91, pp. 7559-7561, May 2001.

[32] M. Yamaguchi; K. Maruta; M. Sugawara; Y. Shimada, "Analysis of Optimum Sheet Resisitance for Integrated Electromagnetic Noise Suppressor," *International Magnetics Conference*, May 2006.

[33] R. C. O'Handley, *Modern Magnetic Material: Principles and Applications*, John Wiley & Sons, INC., 2000.

[34] C. Kittel, "Theory of the Dispersion of Magnetic Permeability in Ferromagnetic Materials at Microwave Frequencies," *Physical Review*, vol. 70, pp. 281-290, Sept. 1946.

[35] B. Rejaei M. Vroubel, "Suppression of Skin Effect in Metal/Ferromagnet Superlattice Conductors," *Journal of Applied Physics,* vol. 96, num, 11, pp. 6863-6868, Dec. 2004.

[36] B. Bayard, D. Vincent, C. R. Simovski, G.Noyel, "Electromagnetic Study of a Ferromagnetic material Coplanar Isolator Suitable for Integration," *IEEE Trans. Microwave Theory Tech.*, vol. 51, pp. 1809-1814, July 2003.

[37] D. Nghiem, J. T. Williams, D. R. Jackson, A. A, Oliner, "Suppression of leakage on stripline and microstrip structures," Microwave *Symposium Digest*, vol. 1, pp. 145-148, May 1994.

[38] H. K. Song, J. H. Oh, J. C. Lee, S. C. Choi, "Magnetic properties and microstructure of YIG thick films prepared by screen printing," Phys. *Stat. Sol.*, vol. 189, No. 3, pp. 829-832, 2002.